RETRACTED: A Synthetic Peptide Designed to Neutralize Lipopolysaccharides Attenuates Metaflammation and Diet-Induced Metabolic Derangements in Mice

Shireen Mohammad[1]*, Sura Al Zoubi[1,2], Debora Collotta[3], Nadine Krieg[4,5], Bianka Wissuwa[4,5], Gustavo Ferreira Alves[3], Gareth S. D. Purvis[1,6], Giuseppe Danilo Norata[7,8,9], Andrea Baragetti[7,8], Alberico Luigi Catapano[7,8,9], Egle Solito[1,10], Elisabeth Zechendorf[11], Tobias Schürholz[11], Wilmar Correa-Vargas[12], Klaus Brandenburg[13], Sina M. Coldewey[4,5], Massimo Collino[14], Muhammad M. Yaqoob[1], Lukas Martin[1,11†] and Christoph Thiemermann[1*†]

[1] William Harvey Research Institute, Bart's and The London School of Medicine and Dentistry, Queen Mary University of London, London, United Kingdom, [2] Department of Basic Medical Sciences, School of Medicine, Al-Balqa Applied University, As-Salt, Jordan, [3] Department of Drug Science and Technology, University of Turin, Turin, Italy, [4] Department of Anesthesiology and Intensive Care Medicine, Jena University Hospital, Jena, Germany, [5] Septomics Research Center, Jena University Hospital, Jena, Germany, [6] Sir William Dunn School Pathology, University of Oxford, Oxford, United Kingdom, [7] Department of Pharmacological and Biomolecular Sciences, University of Milan, Milan, Italy, [8] IRCCS Multimedica, Sesto San Giovanni, Milan, Italy, [9] Società Italiana per lo Studio della Aterosclerosi (S.I.S.A.) Centre for the Study of Atherosclerosis, Bassini Hospital, Milan, Italy, [10] Dipartimento di Medicina Molecolare e Biotecnologie Mediche, Universitá degli Studi di Napoli "Federico II", Napoli, Italy, [11] Department of Intensive Care and Intermediate Care, University Hospital RWTH Aachen, Aachen, Germany, [12] Forschungszentrum Borstel, Department of Biophysics, Borstel, Germany, [13] Brandenburg Antiinfektiva GmbH, c/o Forschungszentrum Borstel, Borstel, Germany, [14] Department of Neurosciences "Rita Levi Montalcini", University of Turin, Turin, Italy

Metabolic endotoxemia has been suggested to play a role in the pathophysiology of metaflammation, insulin-resistance and ultimately type-2 diabetes mellitus (T2DM). The role of endogenous antimicrobial peptides (AMPs), such as the cathelicidin LL-37, in T2DM is unknown. We report here for the first time that patients with T2DM compared to healthy volunteers have elevated plasma levels of LL-37. In a reverse-translational approach, we have investigated the effects of the AMP, peptide 19-2.5, in a murine model of high-fat diet (HFD)-induced insulin-resistance, steatohepatitis and T2DM. HFD-fed mice for 12 weeks caused obesity, an impairment in glycemic regulations, hypercholesterolemia, microalbuminuria and steatohepatitis, all of which were attenuated by Peptide 19-2.5. The liver steatosis caused by feeding mice a HFD resulted in the activation of nuclear factor kappa light chain enhancer of activated B cells (NF-κB) (phosphorylation of inhibitor of kappa beta kinase (IKK)α/β, IκBα, translocation of p65 to the nucleus), expression of NF-κB-dependent protein inducible nitric oxide synthase (iNOS) and activation of the NOD-, LRR- and pyrin domain-containing protein 3 (NLRP3) inflammasome, all of which were reduced by Peptide 19-2.5. Feeding mice, a HFD also resulted in an enhanced expression of the lipid scavenger receptor cluster of differentiation 36 (CD36) secondary to activation of extracellular signal-

regulated kinases (ERK)1/2, both of which were abolished by Peptide 19-2.5. Taken together, these results demonstrate that the AMP, Peptide 19-2.5 reduces insulin-resistance, steatohepatitis and proteinuria. These effects are, at least in part, due to prevention of the expression of CD36 and may provide further evidence for a role of metabolic endotoxemia in the pathogenesis of metaflammation and ultimately T2DM. The observed increase in the levels of the endogenous AMP LL-37 in patients with T2DM may serve to limit the severity of the disease.

INTRODUCTION

Obesity and type-2 diabetes mellitus (T2DM) are associated with metabolic endotoxemia, which has shown to play a key role in the pathophysiology of diabetes. The leak of lipopolysaccharide (LPS) underlying metabolic endotoxemia is due to changes in the gut microbiota (1). Under physiological conditions, the gut epithelium is an efficient barrier, but many factors, such as dietary alterations can lead to changes to the intestinal epithelium. The membrane becomes 'leaky' allowing LPS to enter the bloodstream. This increase in plasma LPS in response to dietary alterations is termed metabolic endotoxemia (2). Once LPS has entered the bloodstream it can activate Toll-like receptor-4 (TLR4), resulting in low-grade systemic inflammation (3).

In 2007, Cani and colleagues were the first to define metabolic endotoxemia as a 2-3-fold increase in the level of plasma LPS due to dietary alterations, ultimately leading to low-grade inflammation and the development of cardiometabolic diseases. Mice-fed a high-fat diet (HFD) for four weeks to induce metabolic endotoxemia, showed similar levels of serum LPS to that of mice infused with LPS continuously for four weeks (4). It should be noted that the levels of LPS demonstrated due to a HFD are 10-15 times lower than the levels seen in humans or animals with sepsis (4). Indeed, metabolic endotoxemia causes low grade inflammation, while the release of large amounts of LPS in sepsis causes a profound degree of systemic inflammation driven by a 'cytokine storm'.

The hypothesis that endotoxin is the driver of the key metabolic changes associated with obesity and diabetes is still controversial (5). TLR4 knock-out mice, fed a HFD demonstrated less insulin resistance and presented an improved glucose tolerance test compared to wild-type mice (6, 7). Atherosclerosis-prone apolipoprotein E-deficient (ApoE$^{-/-}$) mice deficient in either TLR4 or myeloid differentiation primary response 88 (MyD88) develop less atherosclerosis (8). On the other hand, the determination of LPS relies on the limulus amebocyte lysate (LAL) assay, which is used to detect endotoxins, however, this assay has several limitations [reviewed in (9)]. In addition, elevated levels of LPS have also been reported in healthy volunteers. Thus, further studies are warranted which provide evidence that interventions, which prevent either the development of metabolic endotoxemia or its effects reduce the pathology of metaflammation.

Antimicrobial peptides (AMPs) were identified nearly 100 years ago and they are an important part of innate immunity (10). LL-37 is the only human member of the cathelicidin family of AMPs. The role of LL-37 (also known as CRAMP) in murine models of diet-induced obesity is controversial as both beneficial and detrimental effects have been reported: For example, the overexpression of LL-37 in mice prevents diet-induced increases in cluster of differentiation 36 (CD36) expression, hepatic steatosis and obesity (11). In contrast, when mice in which the gene for CRAMP (LL-37) has been deleted (Cramp$^{-/-}$ mice), are fed a HFD, they gain less weight and show a higher insulin sensitivity then WT mice challenged with the same diet. In addition, Cramp$^{-/-}$ mice have lower counts of myeloid cells, monocytes and neutrophils in their adipose tissue (12). The role of LL-37 in humans with diabetes and/or obesity is not known.

LL-37 cannot be utilized as a therapeutic intervention, as high doses of this peptide have substantial neuro-and nephrotoxicity (13). Thus, synthetic AMPs, such as peptide 19-2.5, were developed with reduced toxicity as a potential lead candidate for the treatment of diseases in which AMPs may be useful including T2DM. Peptide 19-2.5 was designed to have a maximal binding capacity for the lipid-A moiety of LPS and to neutralize LPS and has shown to attenuate effectively both systemic inflammation and organ injury/dysfunction which is associated with sepsis. This is achieved by the peptide being able to bind to and inactive LPS (14, 15).

Here, we have investigated the levels of LL-37 in healthy volunteers and in patients with T2DM. Having found that T2DM is associated with a significant increase in LL-37, we have evaluated the effects of the LL-37 mimetic Peptide 19-2.5 in a HFD-induced, murine model of T2DM. Specifically, we investigate the effects of Peptide 19-2.5 on the increase in insulin resistance, hypercholesterolemia, steatohepatitis and proteinuria (microalbuminuria) caused by HFD and use both molecular and metabolomics approaches to gain a better insight into its mechanism of action.

METHODS

Ethical Statement

All animal protocols in this study were approved by the Animal Use and Care Committee of Queen Mary University of London (QMUL), in accordance with the Home Office Guidance on the Operation of Animals (Scientific Procedure Act 1986), published

by Her Majesty's Stationary Office and the Guide for the Care and Use of Laboratory Animals of the National Research Council and were approved by the Animal Welfare Ethics Review Board of QMUL. All research was conducted under the U.K. home office project license number: 70/8350. Human samples for LL-37 determination were obtained from subjects participating in the Progressione delle Lesioni Intimali Carotidee (PILC) project, which has been extensively described elsewhere (16–18). Subjects of this study were screened at the Center for the Study of Atherosclerosis at E. Bassini Hospital (Cinisello Balsamo, Milan, Italy) for personal and familial clinical history of T2DM [defined according to validated criteria (19, 20) and as previously described (21)]. The study was approved by the Scientific Committee of the University of Milan (SEFAP/Pr.0003). An informed consent was obtained in accordance with the Declaration of Helsinki.

HFD-Induced, Murine Model of T2DM

Ten-week-old male C57BL/6 mice, weighing 20-30 g (Charles River Laboratories UK Ltd, Kent, UK). Five mice were housed together in ventilated cages (total of 20 mice), all cages were lined with absorbent bedding material under standard laboratory conditions. For environmental enrichment tubes and chewing blocks were placed into each cage. All mice had access to water *ad libitum* and were housed in a temperature-controlled room (20 ± 2°C) and subjected to a 12 h light and dark cycle. Mice were randomly selected to receive either a normal chow diet (20% protein, 9% fat, 4% fiber and 7% simple sugar) purchased from Labdiet® (5R58 picolab mouse diet 20) (St Louis, Missouri, USA) or a HFD (≈ 60% energy from fat) purchased from the laboratory animal nutrition company TestDiet® (58Y1 diet, St Louis, Missouri, USA) for 12 weeks. Every week, the animals were weighed, and the diet was adapted to body weight of each mouse. After 6 weeks of feeding mice a HFD, mice were randomly assigned to either receive vehicle (sterile saline, 0.9% NaCl i.p.) (HFD+Veh, n=20) or the drug treatment, Peptide 19-2.5 (HFD+Pep2.5, n=20) (10 mg/kg x day i.p in vehicle) for 5 days per week from the end of week 6 until the end of the experiment at week 12. Chow-fed mice remained on the chow diet and received vehicle (sterile saline, 0.9% NaCl i.p.) from the end of week 6 until the end of the experiment at week 12.

OGTT

An OGTT was performed after a fasting period of 6 h in all mice at week 6 and 12 (i.e. before intervention and after intervention). Glucose was administered at a concentration of 2 g/kg body weight (bw) dissolved in drinking water and administrated by oral gavage. Mice were placed in a restrainer and a small cut on the side of their tail was made to collect blood to monitor the level of blood glucose at 0, 15, 30, 45, 60, 90 and 120 min from the administration of glucose using a glucose analyzer (Accu-Chek Compact System, Roche Diagnostics, Basel, Switzerland).

Assessment of Renal Function

At week 12, mice were individually placed in metabolic cages with free access to food and water for 24 h to collect urine

samples. Urine volume (urine output) was measured at the end of the 24 h. Urine creatinine was measured in a blinded fashion by a commercial veterinary testing laboratory (MRC Harwell Institute, Oxfordshire, UK).

Calculating Albumin to Creatinine Ratio

ACR was calculated using equation 1 as a measurement of microalbuminuria.

$$ACR = \frac{Urine\ Albumin}{Urine\ Creatinine}$$

Equation 1. Equation for ACR. ACR is calculated using, urine albumin (mg/dL) and urine creatinine (mg/dL).

ELISA

Commercially available mouse albumin ELISA Kits as per manufactures instructions (Cambridge Bioscience, Cambridge), were used to measure urinary albumin according to the manufacture's instruction. The absorbance read on ELISA plate reader at 450 nm using a spectrofluorometer (Tecan Infinite M200 Pro, Tecan, Austria).

Western Blot Analysis

Immunoblot analyses of liver tissues were carried out using a semi-quantitative western blotting. To assess the degree of phosphorylation of inhibitor of kappa beta kinase (IKK) α/β at $Ser^{176/180}$, the phosphorylation of IκBα at $Ser^{32/36}$, the translocation of the nuclear factor kappa light chain enhancer of activated B cells (NF-κB) p65 subunit (RelA) to the nucleus and the inducible nitric oxide synthase (iNOS) expression. Also, we have evaluated the assembly and activation of the NOD-, LRR- and pyrin domain-containing protein 3 (NLRP3) inflammasome, including activation of caspase-1. The phosphorylation on Ser^{307} of insulin receptor substrate 1 (IRS-1) and the phosphorylation on Ser^{473} of protein kinase B (Akt). Levels of CD36 expression and the degree of phosphorylation of extracellular signal-regulated kinases 1 and 2 (ERK1/2) at the Thr^{202}/Tyr^{204} and Thr^{185}/Tyr^{187} respectively, were also evaluated in liver samples.

Antibodies were purchased from Cell Signaling Technology, if not stated. The antibody used were (1:1000): rabbit anti-Ser^{307} IRS-1, mouse anti-total IRS-1, mouse anti-Ser^{473} Akt, rabbit anti-total Akt, rabbit anti-$Ser^{176/180}$-IKKα/β, rabbit anti-total IKKα/β, mouse anti-$Ser^{32/36}$-IκBα, mouse anti-total IκBα, rabbit anti-NFκB p65, rabbit anti-iNOS, anti-tubulin (Abcam), rabbit anti NLRP3 inflammasome (Abcam), mouse anti-caspase 1 (p20) (Adipogen), Anti-CD36 (Abcam), rabbit anti-phospho-p44/42 MAPK (ERK1/2), rabbit anti-total p44/42 MAPK (ERK1/2), Anti-β-actin (Sigma-Aldrich, Inc).

Mouse liver tissue weighing 30 mg to prepare the extractions (total and/or cytosol/nucleus extractions), standardized loading 50mg of protein into the well of the gel for each sample. In cold conditions (at 4°C) a 10-time dilution with homogenization buffer (HB:20mM Hepes-KOH pH 7.9; 1mM MgCl 2; 0.5mM EDTA; 1mM EGTA;1% NP-40 (or TRITON-X 100) were used to bring to 100 ml in bi-distilled water and just before use 1ul/ml

DTT; 0.5mM PMSF; 1ul/ml PIC) were added to homogenize the sample to obtain the total extraction protein content. For cytosolic protein extraction, the homogenate was centrifuged (at 1320g, 5 min, 4°C). To obtain the cytosolic fraction the supernatants were removed and centrifuged (at 16125g, 40 min, 4°C). The pellet was discarded, and supernatant was kept at -80°C for cytosolic protein analysis. The first pelleted nuclei were re-suspended in extraction buffer (EB: 20mM Hepes-KOH pH 7.9; 1.5mM MgCl 2; 0.2mM EDTA; 1mM EGTA; 20% Glycerol; 420mM NaCl bring to 50 ml in bi-distilled water and just before use were added: 1ul/ml DTT; 0.5mM PMSF; 1ul/ml PIC) at concentration 1/3 compared to the HB) and kept in ice for 30 min, vortexing occasionally, before being centrifuged (at 16125g, 20 min, 4°C). The resulting supernatant was kept at -80°C for nuclear protein analysis later. Both cytosolic/nuclear fraction protein content were determined using bicinchoninic acid (BCA) protein assay following manufacturer's directions (Therma Fisher Scientific, Rockford, IL, USA). Proteins were separated by gel electrophoresis using 8% sodium dodecyl sulphate-polyacrylamide (SDS-PAGE) then transferred into a Polyvinyldenedifluoride (PVDF) membrane, blocked using 10% milk solution in tris-buffered saline with 0.1% Tween 20 detergent (TBST) then the membrane was incubated with a primary antibody (1:1000) in TBS1X at 4°C. The next day, the blots were washed 3 times for 15 min and incubated with HRP-conjugated anti-rabbit or anti-mouse secondary antibody diluted 1:10,000 in 5% blocking solution at room temperature for 30 min. Then the membranes were washed 3 times for 15 min and the protein bands were visualized using enhanced chemiluminescence (ECL) detection system. Bands analysis was performed using densitometric Gel pro analyzer 4.5, 2000 software (Media Cybernetics, Silver Spring, MD, USA). Results were then adjusted against corresponding chow data.

Organ and Blood Collection

At the end of the experiment mice were anaesthetized with isoflurane (3%) delivered in oxygen (1 L/min). They were then sacrificed by terminal cardiac puncture and exsanguination (removal of blood) with a G25 needle. Approximately 0.7 ml of blood was collected from each mouse and decanted immediately into 1.3 ml serum gel tubes (Sarstedt, Nümbrecht, Germany). All organs were collected and snap frozen in liquid nitrogen and were stored at -80°C. A section of the kidney and liver were placed in 2-methylbutane and then transferred to liquid nitrogen and stored at -80°C. A section of the kidney and liver were fixed in formalin for 48 h and was then transferred to 70% ethanol for long-term storage. The rest of the organ collected and placed in liquid nitrogen and were stored at -80°C. Blood serum was isolated after being centrifuged for 3 min at 9900 rpm, snap frozen in liquid nitrogen and stored at -80°C. 100 μl of serum samples were then analyzed in a blinded fashion by a commercial veterinary testing laboratory (MRC Harwell Institute, Oxfordshire, UK) to evaluate the following biomarker: total cholesterol, triglycerides, glucose (non-fasting) and alanine aminotransaminase (ALT).

Histological Analysis
Oil Red O Staining

Oil Red O staining was used for the visualization of fat in liver samples. Frozen liver samples (using 2-methyl butane) were embedded in optimal cutting temperature compound (OCT), and cut into 10 μm sections. Frozen liver sections were left out for 10 min to bring to room temperature. For 5 min, the sections were fixed in 10% neutral buffered formaldehyde, followed by the samples being rinsed thoroughly with running tap water. Sections were then saturated with Oil Red O (1% w/v,60% isopropyl alcohol) (Sigma-Aldrich, Inc., St. Louis, Missouri, USA) and left to incubate for 15 min, then washed twice with 60% isopropyl alcohol solution, followed by being rinsed in distilled water. For 2 min, sections were then stained with Mayer's hematoxylin, followed by blue in running tap water. Using coverslips, the sections were mounted using aqueous glycergel mounting medium (Dako, Cambridge, UK).

Picro-Sirius Red Staining

Picro-Sirius Red staining was used for the visualization of collagen in liver samples. Samples were embedded in paraffin and cut into 4 μm sections. Liver sections were deparaffinized by washing twice in xylene for 5 min, then rehydrated by washing in ethanol with decreasing concentrations (100%, 95%, 90%, 80% and 70%) for 5 min. Sections were then washed in distilled water for 5 min. Picro-Sirius stain (Abcam®, Cambridge, UK), was then covered completely over the sections and incubated in the dark for 60 min. Slides were then rinsed quickly in two changes of 0.5% acetic acid solution. Slides were then dehydrated by being rinsed in two changes of absolute alcohol (100% ethanol) for 10 min. Slides were cleared with d-limonene (national diagnostic®, Nottingham, UK) and mounted in synthetic resin (distyrene, plasticizer and xylene (DPX) mountant) using coverslips.

Slides from both Oil Red O and Picro-Sirius Red were scanned using a NanoZoomer Digital Pathology Scanner 2.0HT (Hamamatsu Photonics K.K, Hamamatsu, Japan) to obtain high-resolution images for analysis. Ten fields were then selected from each image randomly at 40x magnification to quantify lipids from Oil Red O staining and collagen from Picro-Sirius Red staining in the liver were analyzed using the NDP viewer software. The percentage of fat deposition and collagen in the liver were calculated using the ImageJ software version 3.3.2.

LL-37 Measurement

A commercial human LL-37 ELISA kit (#MBS2512823; MyBioSource, San Diego, California, USA) was used to analyze the concentration of LL-37 in healthy subjects and patients with T2DM (**Table S1**). According to the detection range 1.563-100 ng/ml of the ELISA kit the samples were diluted 1:20 in sample diluent. The measurement was performed in accordance with the manufacturer's instructions. The 332 optical density was measured at 450 nm using iMark™ Microplate Absorbance Reader (Bio-Rad Laboratories, Inc).

Bio-Plex Pro Mouse Chemokine Assay

Cytokines, chemokines and growth factors were quantified in murine serum samples using Bio-Plex Pro™ Mouse Chemokine 31-Plex panel assay (Bio-Rad Laboratories, Inc., Hercules, California, USA). The cytokines IL−2, -6, −10, −16, CCL2, -5. The chemokines CXCL1, CX3CL1, -12 – 13 -16, and the growth factor GM-CSF were measured according to the manufacturer's instructions. Data was acquired on Bio-Plex® 200 system (Bio-Rad Laboratories, Inc).

Metabolomic Analysis

Metabolites were analyzed by liquid chromatography coupled to triple quadrupole mass spectrometry (LC-MS/MS) using a high-performance liquid chromatography (HPLC) system (Prominence series) with an inert kit and the triple quadrupole mass spectrometer LCMS-8050, both from Shimadzu Deutschland GmbH (Duisburg, Germany). Samples were then analyzed with the sphingosine-1-phosphate (S1P)/sphingosine method and the supplied method packages "primary metabolites", "phospholipids" and "lipid mediators" according to the manufacturer's protocols (Shimadzu Deutschland GmbH, Duisburg, Germany) with the following modifications: 20 µl of serum sample were precipitated by addition of 200 µL of methanol (LCMS-grade) in vials. Prior to processing, the methanol was spiked with internal standard (IS) solution in a final concentration of 9.09 µM 2-morpholinoethanesulfonic acid (Sigma-Aldrich, Inc.), 136.36 nM lysophosphatidylcholine (17:0) (Sigma-Aldrich, Inc.) and 136.36 nM sphingosine (17:0) (Cayman Chemical, Michigan, USA). After 4 days of incubation the supernatant was analyzed at -80°C and centrifugation at 14,000 g for 10 min at 4°C. Primary metabolites were analyzed using the HPLC Column Discovery® HS F5, 3 µm, 150 mm x 2.1 mm (Sigma-Aldrich, Inc). For phospholipids and lipid mediators the 2.1 x 150 mm 2.6 µm particle size C8 Kinetex LC Column (Phenomenex, Inc., Torrance, USA) was used. Sphingosine-1-phosphate and sphingosine were separated using a MultoHigh 100 RP 18-3µ 60 x 2 mm column (Chromatography Service GmbH, Langerwehe, Germany) with intermittent runs for equilibration. Mass spectrometric detection was performed by multiple reactions monitoring (MRM) after injection of 10 µl sample, unless stated otherwise. Further information on HPLC programs and solvents (**Table S2**), LCMS-8050 settings (**Table S3**), and recorded mass transitions of identified significantly changed analytes (**Tables S4–S7**). Metabolome primary data were analyzed and further processed with LabSolutions 5.91 and LabSolutions Insight 3.10 (Shimadzu Deutschland GmbH).

Statistical Analysis

All data were analyzed using GraphPad Prism 7.0 (GraphPad Software, San Diego, California, USA). All data in both text and figures are expressed as mean ± standard error of the mean (SEM) of *n* observations, where *n* represents the number of animals studied. Data was then assessed using One-way or Two-way ANOVA, followed by Bonferroni's *post-hoc* or Kruskal-Wallis test and Dunn's multiple comparisons test according to the data distribution profile. A two-tailed unpaired student t-test was performed when the mean of two experimental groups were compared. P< 0.05 were considered to be statistically significant.

Statistical outliers were detected by outlier test to analyze the statistical significance of the LL-37 concentration in patients and sample valves were interpolated from 4PL regression standard curve. Area under the curve was used to analyze the OGTT test results. Metabolome data were analyzed by calculating area ratios for each analyte by dividing peak area of each analyte by peak area of the related IS. Data analysis for metabolome data was performed as follows: readings below detection level were set to half of detection level for each analyte separately. Metabolome data was log2 transformed and normalized by subtracting median metabolite abundance per sample from all abundances of each sample. Normalization was carried out separately for primary metabolites (included S1P and sphingosine), phospholipids and lipid mediators. Z scores were calculated using mean and standard deviation of all samples. Contrasts were analysed pairwise between all three sample groups (chow, HFD+Veh, HFD+Pep2.5) by unpaired t-tests. P-values were Benjamini Hochberg adjusted (22). Data analysis was carried out using R version 3.4.4 (R Core Team 2018). R: A Language and Environment for Statistical Computing. Vienna: R Foundation for Statistical Computing', available online at: https://www.R-project.org/.

RESULTS

LL-37 Is Increased in Patients With T2DM

When compared to healthy subjects, LL-37 concentration was significantly higher in patients with T2DM (**Figure 1**).

Treatment With Peptide 19-2.5 Attenuates Weight Gain and Insulin Resistance in High-Fat Diet-Fed Mice and Improves Insulin Signaling in the Liver

When compared to chow-fed mice, HFD-fed mice treated with vehicle had a higher body weight throughout the experiment (**Figure 2A**). However, when compared to HFD-fed mice treated with vehicle, HFD-fed mice treated with Peptide 19-2.5, significantly attenuated the increase in weight gain from the start of drug treatment (from the end of week 6) until the end of the experiment (week 12) (**Figure 2A**), indicating the effectiveness of Pe2.5 to attenuate the increase in body weight caused feeding mice a HFD. Treatment of HFD-mice with Peptide 19-2.5 (week 6-12) caused a transient reduction in calorie and food intake (at week 8), but neither calorie nor food intake were reduced at the end of the experiment (when compared to HFD-mice treated with vehicle; **Figure S1**).

When compared to chow-fed mice, HFD-fed mice treated with vehicle challenged with an oral dose of glucose developed a significant change in OGTT by 6-weeks of being fed a HFD (**Figure S2**), and this further declined by the end of the
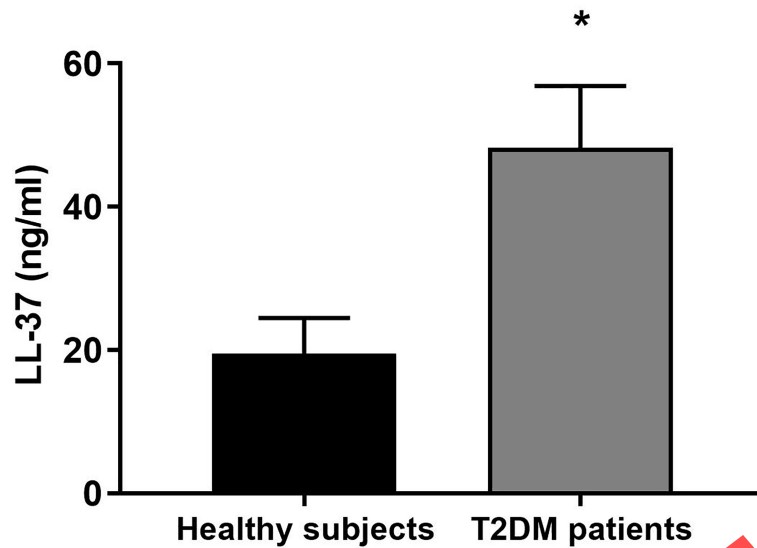
FIGURE 1 | LL-37 serum levels in healthy subjects and patients with T2DM. Serum concentrations of LL-37 were assessed in healthy subjects and patients with T2DM. Data were analyzed by unpaired t-test (two-tailed). Data are expressed as mean ± SEM; healthy subjects (n = 10), T2DM patients (n = 12). *P < 0.05 *vs.* healthy subjects.

experiment (**Figures 2C, D**). This impairment in OGTT was associated with significantly elevated levels of non-fasting blood glucose level by week 12 (**Figure 2B**) indicating that feeding mice a HFD effectively caused the onset of hyperglycemia. However, HFD-fed mice treated with Peptide 19-2.5 markedly reduced (i) the impairment in OGTT (**Figures 2C, D**) and the (ii) non-fasting blood glucose levels by week 12 (**Figure 2B**). To gain a better insight into the potential mechanism underlying the reduced insulin resistance after HFD feeding, we investigated the effects of Peptide 19-2.5 on the insulin signaling pathway in the liver. HFD-fed mice treated with vehicle exhibited a significant increase in the phosphorylation on Ser[307] of IRS-1 (**Figure 2E**), hence resulting in a reduction in the phosphorylation of the downstream mediator Akt on Ser[473] (**Figure 2F**), indicating an impairment in insulin signaling. In contrast, treatment with Pep9-2.5 prevented the increase in the phosphorylation on Ser[307] of IRS-1 and hence attenuated the decline in the phosphorylation of Akt on Ser[473], hence, Peptide 19-2.5 effectively improved insulin signaling and glycemic regulation in HFD-fed mice (**Figures 2E, F**).

Treatment With Peptide 19-2.5 Attenuates Hypercholesterolemia in High-Fat Diet-Fed Mice

When compared to chow-fed mice, HFD-fed mice treated with vehicle showed a significant increase in serum total cholesterol (**Figure 3A**) and a trend of an increase, although not significant in serum triglycerides (**Figure 3B**) suggesting that feeding mice a HFD causes hypercholesterolemia. When compared to HFD-fed mice treated with vehicle, HFD-fed mice treated with Peptide 19-2.5, showed a significant reduction in serum total cholesterol (**Figure 3A**) and a trend of a small, but not significant reduction

in serum triglycerides (**Figure 3B**), demonstrating the ability of Peptide 19-2.5 to attenuate the development of hypercholesterolemia.

Treatment With Peptide 19-2.5 Attenuates Microalbuminuria in High-Fat Diet-Fed Mice

ACR was calculated to study the effect of proteinuria in HFD-fed mice, which is the hallmark symptom of diabetic nephropathy (23, 24). When compared to chow-fed mice, HFD-fed mice treated with vehicle demonstrated a significant increase in ACR by the end of the experiment, indicating the development of microalbuminuria, which was significantly attenuated by the treatment with Peptide 19-2.5 in HFD-fed mice (**Figure 4**).

Treatment With Peptide 19-2.5 Abolishes Steatohepatitis and Liver Injury but Does Not Affect Collagen Deposition in High-Fat Diet-Fed Mice

HFD feeding results in the development of hepatosteatosis (25). When compared to chow-fed mice, HFD-fed mice treated with vehicle showed a significant increase in the percentage of lipids stained with Oil Red O in the liver (**Figure 7B**). However, treatment with Peptide 19-2.5 in HFD-fed mice resulted in a significant reduction in fat deposition in the liver (**Figure 5B**) and, hence, a reduction in steatosis. When compared to chow-fed mice, HFD-fed mice treated with vehicle showed a significant increase in the percentage of collagen fibers in the liver (**Figure 5C**), while treatment with Peptide 19-2.5 in HFD-fed mice showed no significant effect on collagen deposition (**Figure 5C**). HFD-fed mice exhibited an increase in liver weight and a significant increase in serum levels of ALT (liver injury) (**Figure 5D**). Most notably, treatment of HFD-mice with
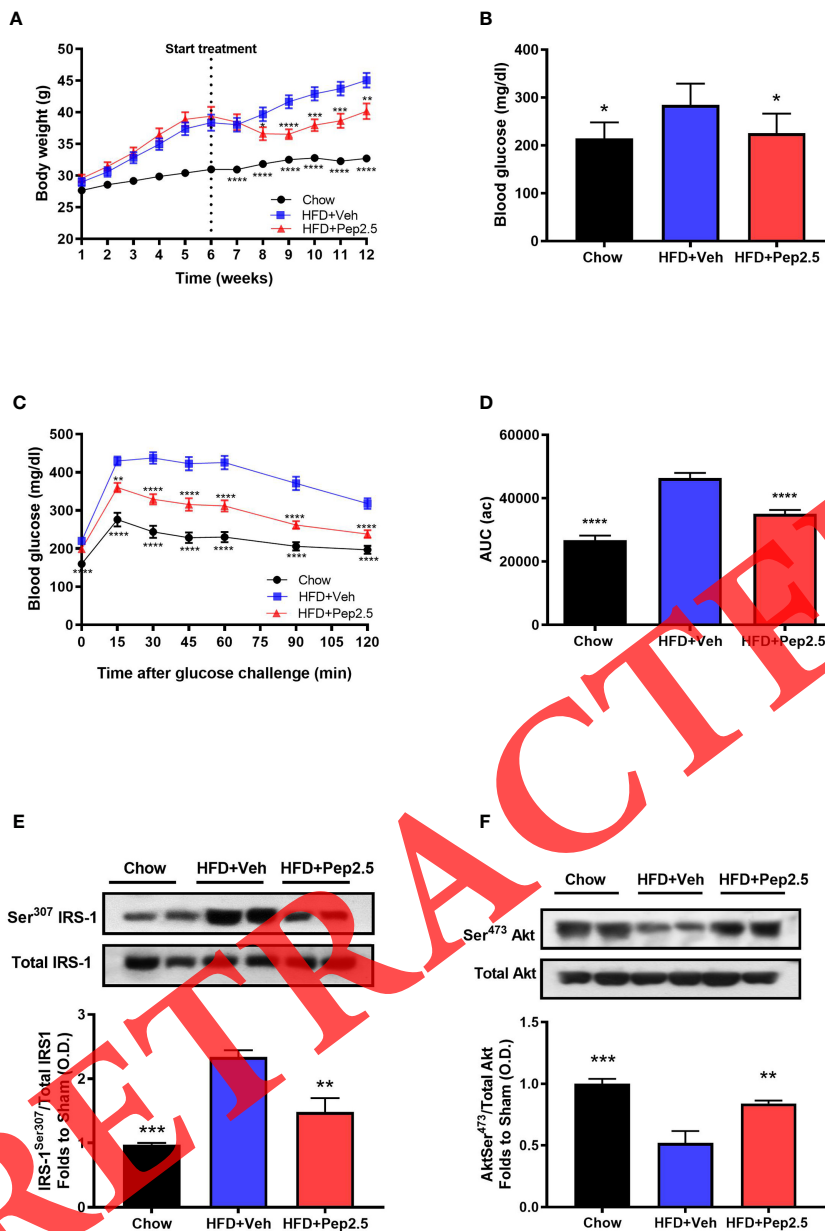
FIGURE 2 | Peptide 19-2.5 ameliorated glycemic regulations by the improvement of insulin signaling in HFD-fed mice. **(A)** Body weight was measured once a week for 12 weeks (g). **(B)** Non-fasting glucose levels were measured at week 12 (mg/dl) **(C)** Oral glucose tolerance (OGTT) was assessed over 120 min, after receiving an oral dose of glucose at week 12 (mg/dl) and the **(D)** area under the curve (AUC) of OGTT was calculated for respective groups and used for statistical analysis (au). Data are expressed as mean ± SEM; n = 20 per group, n = 10 for non-fasting glucose levels. *$P < 0.05$, **$P < 0.01$, ***$P < 0.001$, and ****$P < 0.0001$ *vs.* HFD + Veh. **(E)** Densitometric analysis of the bands is expressed as relative optical density (O.D.) for the phosphorylation on Ser[307] IRS-1 in the liver and normalized to total IRS-1 and **(F)** for the phosphorylation on Ser[473] of Akt in the liver normalized to total Akt. Data was analyzed by one-way ANOVA, with Bonferroni *post-hoc* test. Data are expressed as mean ± SEM; chow (n = 5), HFD+Veh (n = 6), HFD+Pep2.5 (n = 6). **$P < 0.01$ and ***$P < 0.001$ *vs.* HFD+Veh.

Peptide 19-2.5 reduced the increase in liver weight and liver injury caused by the HFD (**Figures 5A, D**). Hence, feeding mice a HFD resulted in the development of a larger fatty liver (steatosis) associated with liver injury, both of which were abolished by treatment of Peptide 19-2.5 in HFD-fed mice.

Treatment With Peptide 19-2.5 Reduces Liver Inflammation in High-Fat Diet-Fed Mice

Using western blot analysis, the NF-κB signaling pathway and the activation of the NLRP3 inflammasome were investigated in
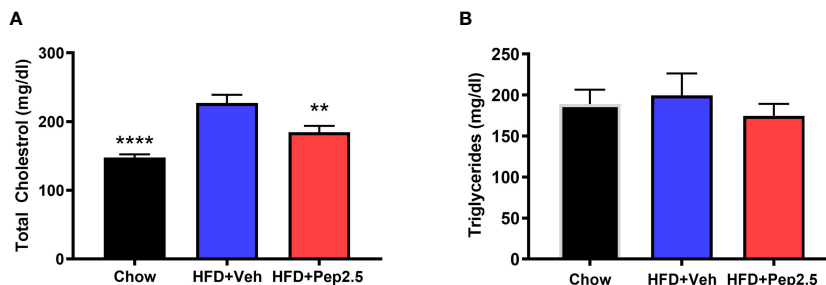
FIGURE 3 | Peptide 19-2.5 attenuates hypercholesterolemia in HFD-fed mice. Serum samples were collected at the end of the experiment to measure **(A)** total cholesterol (mg/dl) and **(B)** triglycerides (mg/dl). Data was analyzed by one-way ANOVA, with Bonferroni *post-hoc* test. Data are expressed as mean ± SEM; n = 10 per group. **P < 0.01 and ****P < 0.0001 *vs.* HFD + Veh.
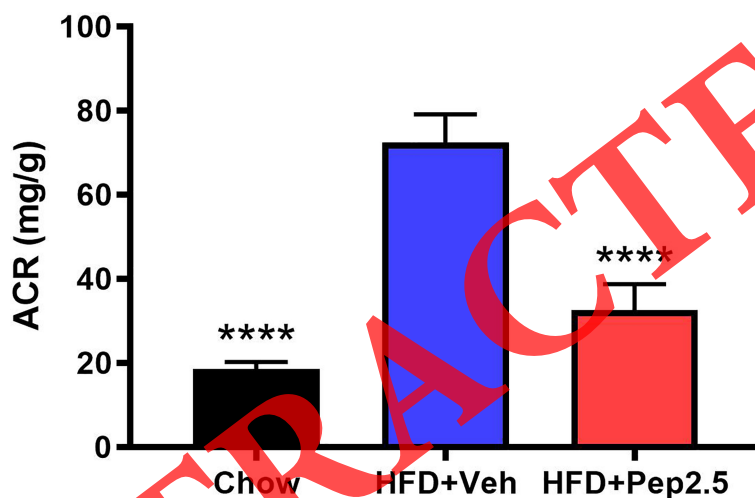
FIGURE 4 | Peptide 19-2.5 attenuates the development of microalbuminuria in HFD-fed mice. At week 12 urine was collected to calculate the albumin to creatinine ratio (ACR) (mg/dl). Data was analyzed by one-way ANOVA, with Bonferroni's *post-hoc* test. Data are expressed as mean ± SEM; n = 10 per group. ****P < 0.0001 *vs.* HFD+Veh.

the liver. Both of which are key drivers of liver inflammation associated with steatohepatitis.

When compared to chow-fed mice, HFD-fed mice treated with vehicle showed a significant increase in the phosphorylation of IKKα/β at Ser$^{176/180}$, in the phosphorylation of IκBα at Ser$^{32/36}$, in the translocation of NF-κB subunit p65 to the nucleus and in iNOS expression in the liver, indicating that feeding mice a HFD causes the activation of the NF-κB signaling pathway (**Figures 6A–D**). Administration of Peptide 19-2.5 in HFD-fed mice significantly attenuated the degree of phosphorylation of IKKα/β at Ser$^{176/180}$, the phosphorylation of IκBα at Ser$^{32/36}$, translocation of the p65 subunit of NF-κB to the nucleus and iNOS expression in the liver (**Figures 8A–D**), indicating the ability of Peptide 19-2.5 to effectively inhibit the NF-κB signaling pathway in the liver.

When compared to chow-fed mice, HFD-fed mice treated with vehicle showed a significant increase in the expression of the inflammasome, NLRP3 and cleavage of pro-caspase-1 to caspase-1 in the liver (**Figures 6E, F**). However, the activation

of assembly of the NLPR3 inflammasome was effectively attenuated by the treatment with Peptide 19-2.5 in HFD-fed mice (**Figures 6E, F**).

Hence, together demonstrates the ability of Peptide 19-2.5 to attenuate the activation of NF-κB as well as the activation and assembly of the NLRP3 inflammasome. Therefore, reducing liver inflammation in HFD-fed mice.

Treatment With Peptide 19-2.5 Reduces the Expression of CD36 and the Activation of ERK in the Liver of High-Fat Diet-Fed Mice
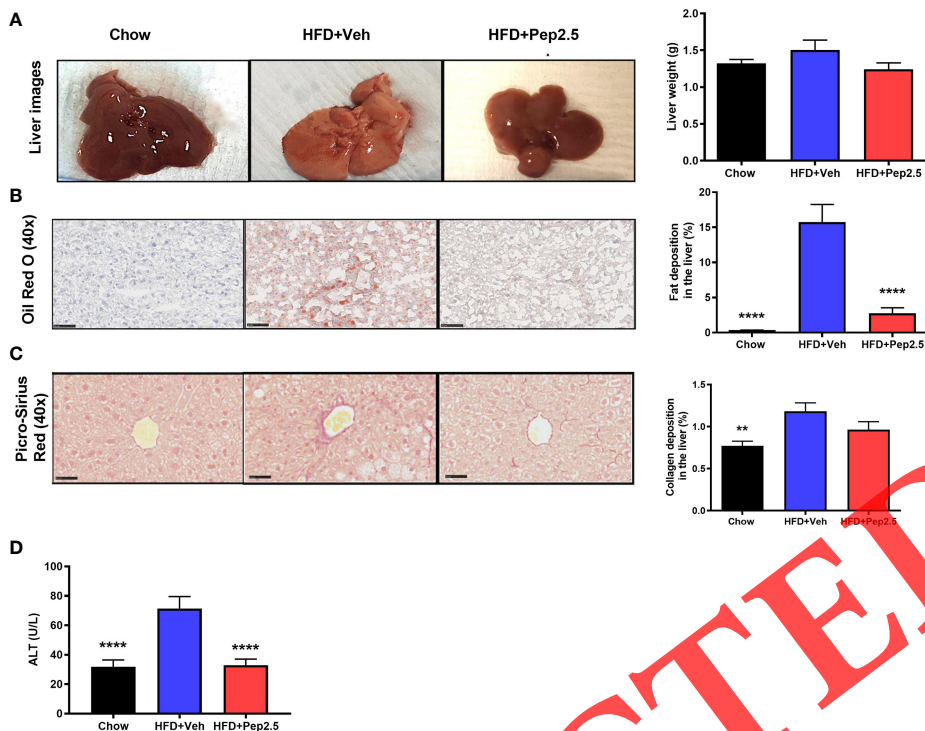
When compared to chow-fed mice, HFD-fed mice treated with vehicle showed a significant increase in the expression of CD36 and the phosphorylation of ERK1/2 (**Figure 7**). However, treatment with Peptide 19-2.5 inhibited the expression of CD36 and the phosphorylation of ERK2, with a small but not

FIGURE 5 | Peptide 19-2.5 abolishes steatohepatitis in HFD-fed mice. **(A)** Liver images of mice immediately after being culled and the liver weights (g). **(B)** Images of hepatic lipid deposition using Oil Red O staining and quantified as percentage of fat deposition (%). **(C)** Images of hepatic collagen deposition using Picro-Sirius Red stain to quantify percentage collagen deposition (%). Insert images are 40x magnification digital zoom and scale bars measure 50μm. **(D)** Serum ALT (U/L). Data were analyzed by one-way ANOVA, with Bonferroni's *post-hoc* test. Data are expressed as mean ± SEM; n = 20 per group. **P < 0.01 and ****P < 0.0001 *vs.* HFD+Veh.

significant reduction of the phosphorylation of ERK1 in the liver in HFD-fed mice (**Figure 7**).

Effect of Peptide 19-2.5 Treatment on Cytokine, Chemokine, and Growth Factor Analysis in High-Fat-Diet-Fed Mice
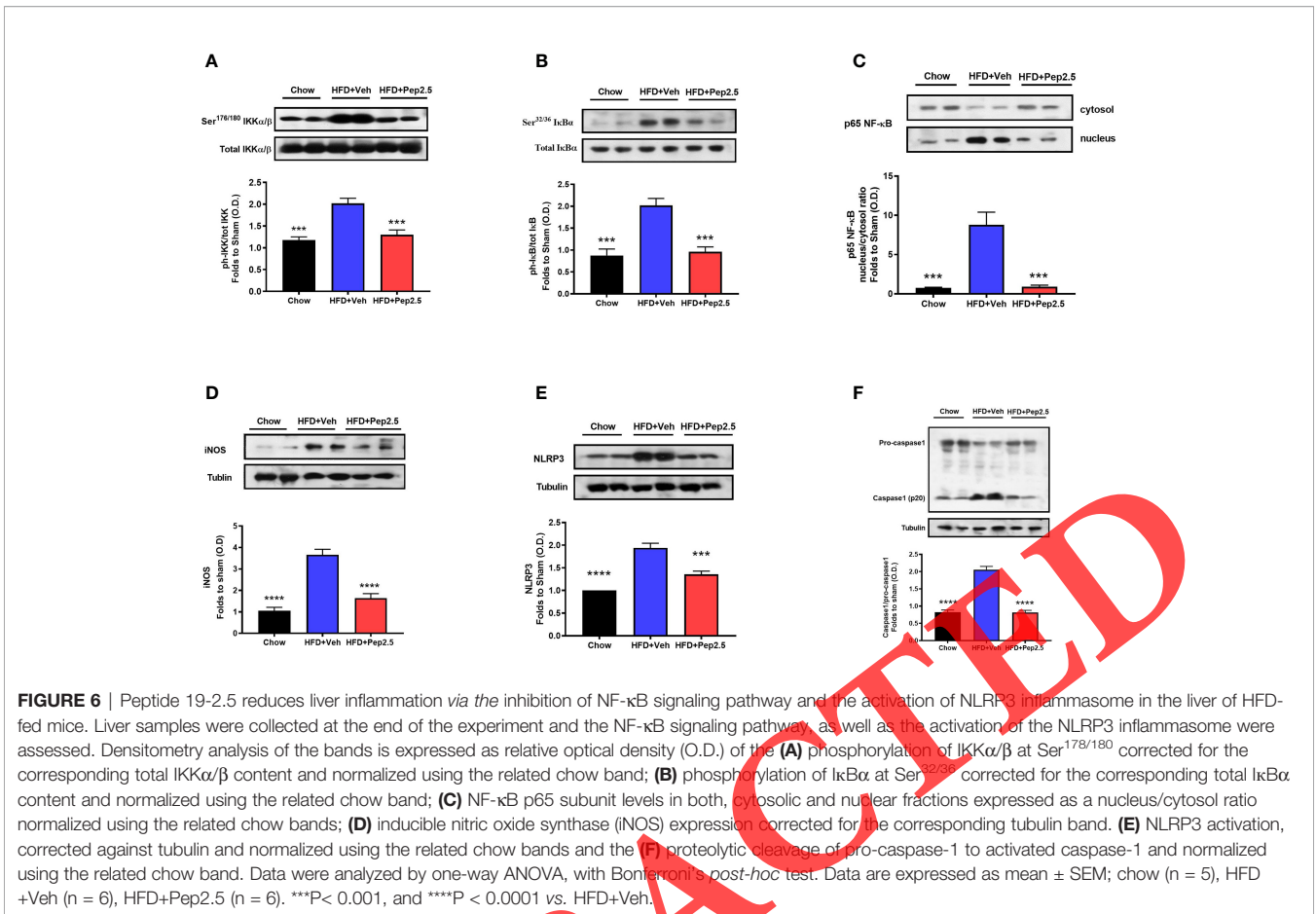
HFD-fed mice treated with peptide 19-2.5, showed no significant differences in the levels of the following cytokines: IL-6, IL-10, IL-16, IL-2, KC/CXCL1, MCP-1/CCL2 and Rantes/CCL5. The following chemokines: Fractalkine/CX3CL1, BCA-1/CXCL13, SDF-1α/CXCL12, SCYB16/CXCL16 and the growth factor, GM-CSF (**Figures 8A–L**).

Treatment With Peptide 19-2.5 Enhances Levels of Carnitine in High-Fat-Diet Fed Mice

Using a targeted metabolomic approach, we studied the effect of Peptide 19-2.5 on metabolite levels in the serum of HFD-fed mice. The detected 217 analytes were subdivided in 49 primary metabolites, 146 phospholipids, 20 lipid mediators, sphingosine-1-phophate and sphingosine. Log2 fold change heatmaps showed all detected analytes (**Figures 9A** and **S6**, **S7**). Significantly changed analytes were identified and analyzed *via* dot plot (**Figure 9B**),

hierarchical clustered z score heatmaps (**Figures S3–S5**) and volcano plots (**Figures 9C–E** and **S8**, **S9**). Detailed statistical information of the detectable analytes is shown in **Supplementary Data**.

The log2 fold change heatmap illustrates all detected primary metabolites, sphingosine-1-phosphate and sphingosine (**Figure 9A**). Within these metabolites only carnitine showed a significant decrease in mice-fed a HFD (treated with vehicle) compared with mice-fed a chow diet as well as a significant increase in the HFD+Pep2.5 group compared with the HFD+Veh group (**Figure 9B**). This indicates an involvement of Peptide 19-2.5 in the restoring of carnitine level in mice-fed a HFD. Volcano plot analysis highlights significantly different analytes with at least twofold changed primary metabolites. The comparison of primary metabolites between the chow group and the HFD+Veh group showed that 5 primary metabolites were significantly reduced in the HFD+Veh group (**Figure 9C**). Seven primary metabolites were significantly decreased and 3 were significantly increased in the HFD+Pep2.5 group compared with chow group (**Figure 9D**). The group comparison between HFD+Pep2.5 and HFD+Veh identified 1 primary metabolite with a significant decrease and 2 primary metabolites with a significant increase in the HFD+Pep2.5 group (**Figure 9E**).

FIGURE 6 | Peptide 19-2.5 reduces liver inflammation *via the* inhibition of NF-κB signaling pathway and the activation of NLRP3 inflammasome in the liver of HFD-fed mice. Liver samples were collected at the end of the experiment and the NF-κB signaling pathway, as well as the activation of the NLRP3 inflammasome were assessed. Densitometry analysis of the bands is expressed as relative optical density (O.D.) of the **(A)** phosphorylation of IKKα/β at Ser$^{178/180}$ corrected for the corresponding total IKKα/β content and normalized using the related chow band; **(B)** phosphorylation of IκBα at Ser$^{32/36}$ corrected for the corresponding total IκBα content and normalized using the related chow band; **(C)** NF-κB p65 subunit levels in both, cytosolic and nuclear fractions expressed as a nucleus/cytosol ratio normalized using the related chow bands; **(D)** inducible nitric oxide synthase (iNOS) expression corrected for the corresponding tubulin band. **(E)** NLRP3 activation, corrected against tubulin and normalized using the related chow bands and the **(F)** proteolytic cleavage of pro-caspase-1 to activated caspase-1 and normalized using the related chow band. Data were analyzed by one-way ANOVA, with Bonferroni's *post-hoc* test. Data are expressed as mean ± SEM; chow (n = 5), HFD +Veh (n = 6), HFD+Pep2.5 (n = 6). ***P< 0.001, and ****P < 0.0001 *vs*. HFD+Veh.

DISCUSSION

We have discovered that patients with T2DM have elevated levels of the endogenous, AMP LL-37. It is not clear whether this increase in LL-37 contributes to the pathophysiology of the metabolic syndrome or T2DM or whether this increase is a defense mechanism to protect us from the consequences of metabolic endotoxemia (see Introduction). If the latter is the case, then AMPs may be able to reduce the degree of metabolic endotoxemia and, hence, some of the pathology associated with T2DM. It should be noted that LL-37 itself is toxic to human T-lymphocytes and human leukocytes (27). LL-37, has also been shown to be toxic in neonatal rat model of septic shock (28) and, hence, cannot be used as a therapeutic remedy. Over the past years, significant efforts have been made to develop synthetic AMPs which do not have toxic effects. One of these peptides, Peptide 19-2.5, binds to and inactivates LPS and, indeed, other damage-associated molecular patters (DAMPs) including heparan sulphate and high mobility group protein B1 (HMGB1) (29). Peptide 19-2.5 is not toxic in cellular assays (e.g. Jurkat cells, human macrophages, human red blood cells) (14, 30). The maximal tolerated dose (MTD) of Peptide 19-2.5 in a 14-day repeated dosing study in rats is greater than 20 mg/kg/day (K Brandenburg, personal communication).

As Peptide 19-2.5 has a favorable toxicological profile when compared to LL-37, we have investigated whether Peptide 19-2.5 affects the metabolic/diabetic phenotype in a HFD-induced model of obesity and T2DM. We report here for the first time that Peptide 19-2.5 reduces the insulin resistance, hypercholesterolemia, steatohepatitis and microalbuminuria caused by feeding mice a HFD. Peptide 19-2.5 also inhibited the activation of NF-κB and the NLRP3 inflammasome and reduced the expression of CD36 as well as ERK1/2 in the liver.

HFD-fed mice showed a progressive increase in body weight indicating the development of obesity. Indeed, it is well known that even shorter periods of HFD (3 weeks) result in insulin resistance and hyperglycemia in mice (31). In our study, mice fed a HFD for 12 weeks developed severe insulin resistance, as indicated by an increase in the impairment of glucose tolerance [measured by the (OGTT) and an increase in non-fasting blood glucose levels at the end of the experiment (week 12), HFD also caused a significant increase in the phosphorylation of Ser^{307} of IRS-1 (a marker of insulin resistance), which impairs the ability of IRS-1 to activate the phosphatidylinositol 3-kinase-dependent downstream pathway (32). Hence, in our study there was a decline in the phosphorylation of the downstream mediator Akt on Ser^{473} in HFD-fed mice treated with vehicle. The phosphorylation of
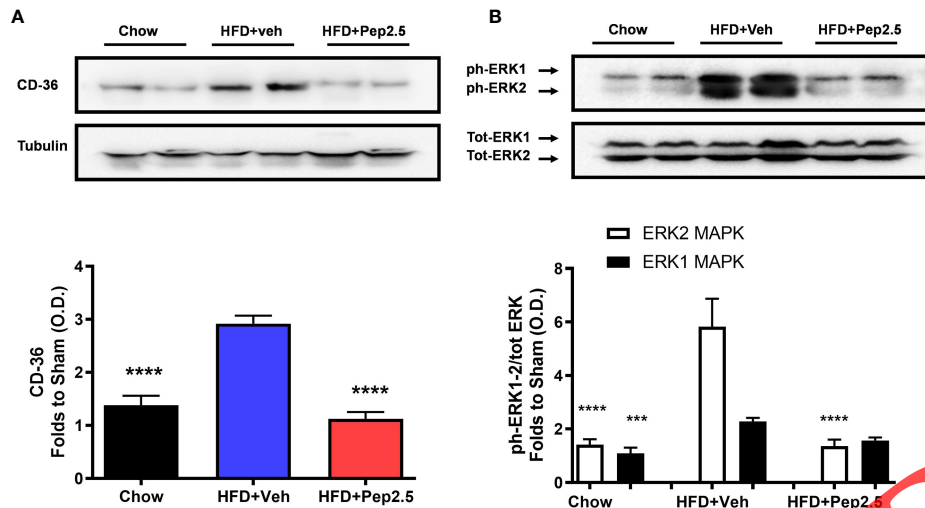
FIGURE 7 | Peptide 19-2.5 reduces CD36 expression and the activation of ERK in the liver of HFD-fed mice. Liver samples were collected at the end of the experiment and the expression of CD36 and the phosphorylation of ERK1/2 were assessed. Densitometry analysis of the bands is expressed as relative optical density (O.D.) of **(A)** CD36 expression, corrected against tubulin and normalized using the related chow bands; **(B)** phosphorylation of ERK1/2 corrected to the corresponding total ERK1/2 content and normalized using the related chow band. Data was analyzed by one-way ANOVA, with Bonferroni *post-hoc* test. Data are expressed as mean ± SEM; n = 8 per group. ***P < 0.001 and ****P < 0.0001 *vs.* HFD+Veh
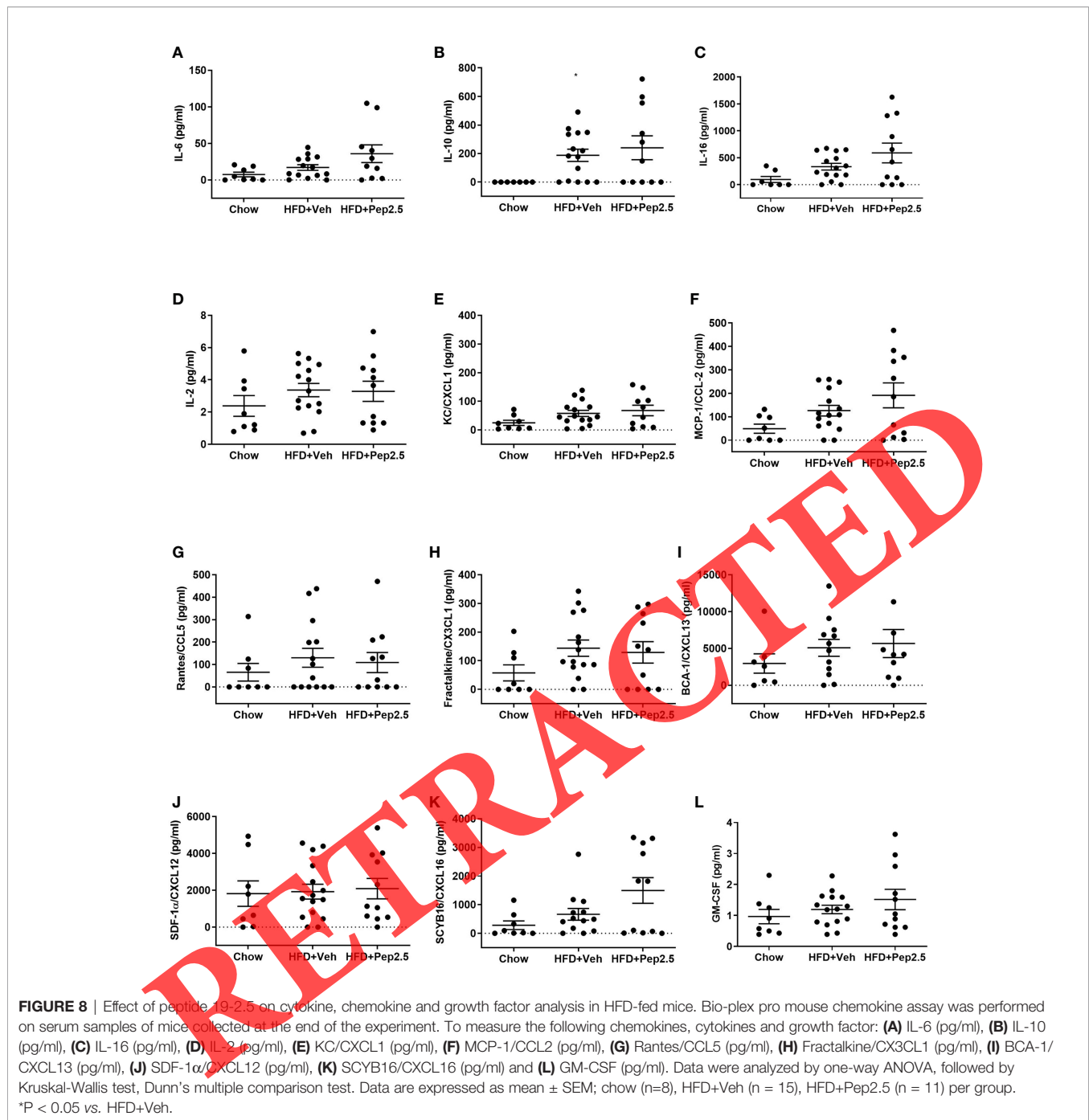
Ser[307] on IRS-1 is also associated with the activation of IKK complex (32). However, the contribution of this in the development of insulin resistance is not well understood. We report here that HFD-fed mice treated with Peptide 19-2.5 resulted in the improvement of glycemic control secondary to the restoration of the IRS-1 signaling pathway in the liver.

One of the hallmarks of diabetic nephropathy in mice and man is the development of (micro) albuminuria (33–35). The elevation in urine albumin, termed microalbuminuria is a result of renal injury and hyperfiltration and is the first sign of diabetic nephropathy which can lead to an increased risk of cardiovascular disease (36). Hyperglycemia is the key driver of the microvascular injury in diabetes, as excess glucose drives the formation of reactive oxygen species (ROS), which in turn activate protein kinase C (PKC) and NF-κB leading to increased expression of vascular endothelial growth factor (VEGF) and vascular permeability (37). ACR is a reliable measure of the development of microalbuminuria (23, 24). We report here that treatment of mice challenged with a HFD and treated with Peptide 19-2.5 (from the end of week 6 to week 12) largely attenuated the microalbuminuria caused by HFD.

The most striking finding of our study, however, is that HFD-fed mice treated with Peptide 19-2.5 abolished steatohepatitis. Exposure of mice to a HFD for 12 weeks resulted in an increase in liver weight secondary to a very dramatic increase in hepatic fat deposition (measured using Oil Red O staining). Indeed, an increase in fat deposition in the liver in response to a HFD occurs as early as 4 weeks in mice (38). This deposition of fat drives steatohepatitis resulting in liver injury (measured as an increase in serum ALT). Most notably, treatment of mice subjected to a HFD for 12 weeks with Peptide 19-2.5 abolished both the

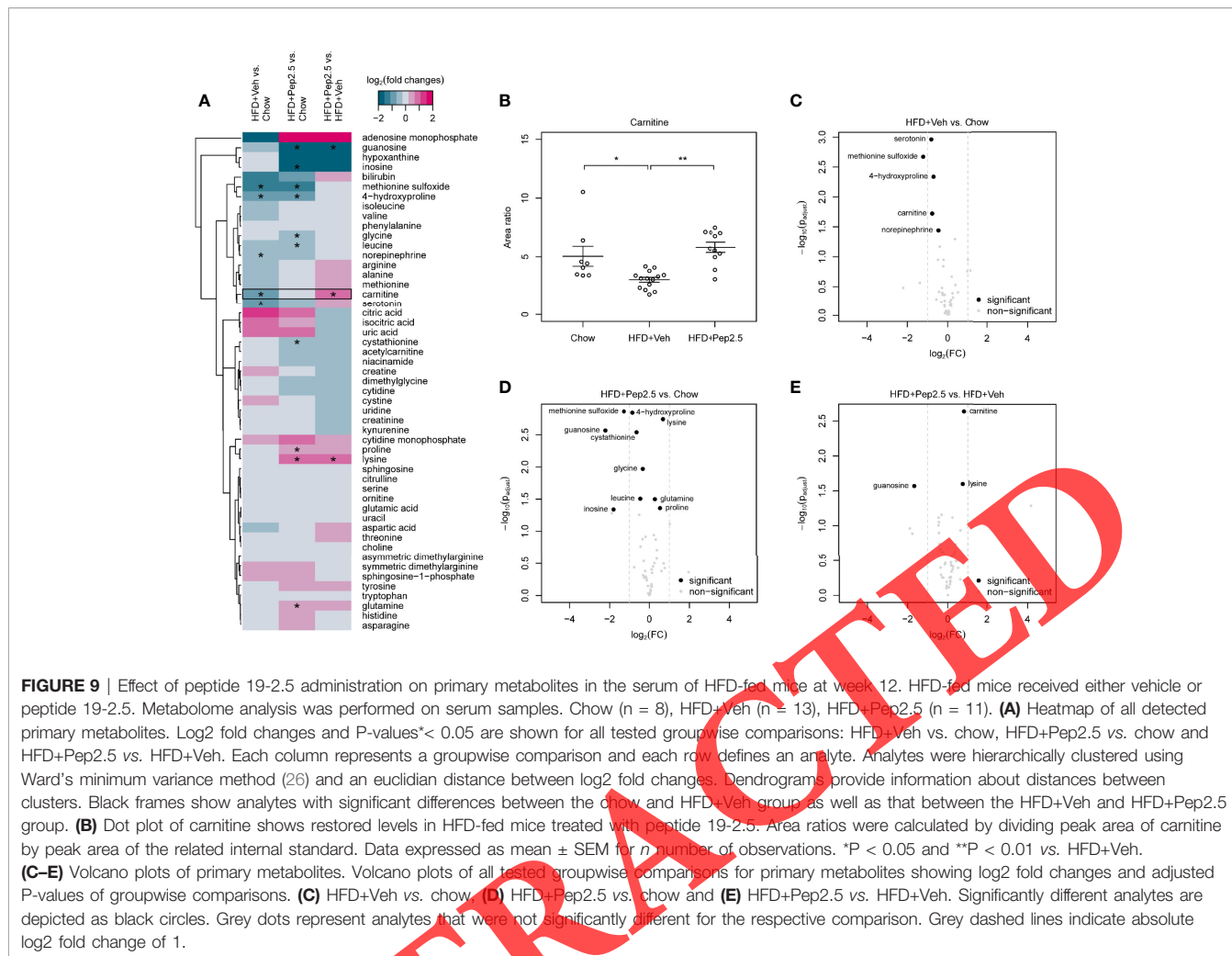increase in liver weight and the degree of fat deposition in mice challenged with a HFD.

The deposition of excessive amounts of fat caused by HFD in the liver was associated with a marked activation of the NF-κB signaling pathway as well as the assembly and expression of the NLRP3 inflammasome, both of which are key drivers of liver inflammation associated with steatohepatitis (39, 40). NF-κB, is a key transcription regulator of the inflammatory response and the activity of NF-κB is regulated by binding to inhibitory units of the IκB proteins, including IκBα, IκB and IκBϵ. IκBα inactivates NF-κB by masking the nuclear localization site of the NF-κB protein and sequestering the inactive NF-κB complex in the cytoplasm. Phosphorylation of IκBα by IKK marks the degradation and the dissociation of IκBα from NF-κB, thus allowing the activated NF-κB to translocate to the nucleus and activate target genes. There is good evidence that NF-κB is essential in regulating the inflammatory signaling pathway in the liver and important for regulating functions in the hepatocytes and Kupffer cells (39, 41, 42), while inhibition of NF-κB reduces the degree of liver injury (43). We report here that mice challenged with a HFD for 12 weeks showed an increase in phosphorylation (a) of IKKα/β on Ser[178/180] and (b) of IκBα at Ser[32/36], (c) in the translocation of NF-κB subunit p65 to the nucleus and (d) the expression of the NF-κB-dependent proinflammatory protein, iNOS in the liver, all of which were attenuated effectively by treatment with Peptide 19-2.5. Indeed, iNOS is widely expressed in many insulin-sensitive tissues/organs including adipose tissue and liver (44). The expression of iNOS is increased in the liver of diabetic mice leading to an impairment in insulin signaling and hyperglycemia, while iNOS inhibition (L-NIL) improves insulin signaling (liver)

FIGURE 8 | Effect of peptide 19-2.5 on cytokine, chemokine and growth factor analysis in HFD-fed mice. Bio-plex pro mouse chemokine assay was performed on serum samples of mice collected at the end of the experiment. To measure the following chemokines, cytokines and growth factor: **(A)** IL-6 (pg/ml), **(B)** IL-10 (pg/ml), **(C)** IL-16 (pg/ml), **(D)** IL-2 (pg/ml), **(E)** KC/CXCL1 (pg/ml), **(F)** MCP-1/CCL2 (pg/ml), **(G)** Rantes/CCL5 (pg/ml), **(H)** Fractalkine/CX3CL1 (pg/ml), **(I)** BCA-1/CXCL13 (pg/ml), **(J)** SDF-1α/CXCL12 (pg/ml), **(K)** SCYB16/CXCL16 (pg/ml) and **(L)** GM-CSF (pg/ml). Data were analyzed by one-way ANOVA, followed by Kruskal-Wallis test, Dunn's multiple comparison test. Data are expressed as mean ± SEM; chow (n=8), HFD+Veh (n = 15), HFD+Pep2.5 (n = 11) per group. *$P < 0.05$ *vs*. HFD+Veh.

and prevents hyperglycemia (44). Most notably, iNOS knock out mice subjected to a HFD develop less insulin-resistance than their wild-type litter mates (45). Thus, prevention of the expression of iNOS (secondary to prevention of the activation of NF-κB) may well have contributed to the beneficial effects of Peptide 19-2.5 observed here.

Activation of the NLRP3 inflammasome in hepatocytes plays a pivotal role in liver disease, while inhibition of the assembly and/or activation of the NLRP3 inflammasome reduces liver inflammation and injury (46, 47). Inflammasomes are cytosolic protein complexes that mediate host immune responses to infection and cellular damage by sensing danger signals *via* NOD-like receptors, NLRs. The assembly of an inflammasome causes the proteolytic cleavage of procaspase-1 into the active caspase-1. The active caspase-1 is important for converting pro-IL-1β into the active IL-1β and the formation of IL-18 amplifying inflammation (48). Here, we demonstrated that Peptide 19-2.5 attenuated the formation of the NLRP3 complex and inhibited the cleavage of pro-caspase 1 to the active caspase caused by HFD in the liver.

FIGURE 9 | Effect of peptide 19-2.5 administration on primary metabolites in the serum of HFD-fed mice at week 12. HFD-fed mice received either vehicle or peptide 19-2.5. Metabolome analysis was performed on serum samples. Chow (n = 8), HFD+Veh (n = 13), HFD+Pep2.5 (n = 11). **(A)** Heatmap of all detected primary metabolites. Log2 fold changes and P-values*< 0.05 are shown for all tested groupwise comparisons: HFD+Veh vs. chow, HFD+Pep2.5 *vs.* chow and HFD+Pep2.5 *vs.* HFD+Veh. Each column represents a groupwise comparison and each row defines an analyte. Analytes were hierarchically clustered using Ward's minimum variance method (26) and an euclidian distance between log2 fold changes. Dendrograms provide information about distances between clusters. Black frames show analytes with significant differences between the chow and HFD+Veh group as well as that between the HFD+Veh and HFD+Pep2.5 group. **(B)** Dot plot of carnitine shows restored levels in HFD-fed mice treated with peptide 19-2.5. Area ratios were calculated by dividing peak area of carnitine by peak area of the related internal standard. Data expressed as mean ± SEM for *n* number of observations. *P < 0.05 and **P < 0.01 *vs.* HFD+Veh. **(C–E)** Volcano plots of primary metabolites. Volcano plots of all tested groupwise comparisons for primary metabolites showing log2 fold changes and adjusted P-values of groupwise comparisons. **(C)** HFD+Veh *vs.* chow, **(D)** HFD+Pep2.5 *vs.* chow and **(E)** HFD+Pep2.5 *vs.* HFD+Veh. Significantly different analytes are depicted as black circles. Grey dots represent analytes that were not significantly different for the respective comparison. Grey dashed lines indicate absolute log2 fold change of 1.

What, then, is the mechanism(s) by which Peptide 19-2.5 reduces the uptake of lipids into the liver? Steatosis is characterized by the accumulation of excess triglycerides in hepatocytes (49). The uptake of fatty acids from the circulation into the liver is dependent on transporters including CD36. CD36 a class B savage receptor which recognizes a variety of ligands including free fatty acids, phospholipids, oxidized low-density lipoprotein (oxLDL) and collagen and is important for fatty acid uptake and lipid metabolism (50). CD36 is highly expressed in many organs associated with diabetes such as the skeletal muscle, cardiac muscle, liver and the kidney. There is good evidence that the CD36 receptor is involved in the pathogenesis of insulin resistance and diabetes (51), as the receptor interacts with glucose, insulin and lipids (52). There is significant evidence that HFD causes an increase in free fatty acids, which results in the upregulation of CD36 in the liver, skeletal muscle, and cardiac muscle, which in turn leads to steatosis and insulin resistance (11, 52, 53). Furthermore, an increase in CD36 expression also positively correlates with the development of non-alcoholic steatohepatitis (NASH) and fatty liver (54). Most importantly, there is evidence that the upregulation of CD36 is a key driver in the pathogenesis of steatosis.

Indeed, hepatocyte-specific CD36 knock out mice challenged with a HFD have a reduction in lipid uptake into the liver and, hence, less steatosis (50). We report here that challenge of mice with HFD leads to an increase in the expression of CD36; and this effect is abolished in HFD-fed mice treated with Peptide 19-2.5. We also report here that the plasma levels of the human cathelicidin, LL-37, are elevated in patients with T2DM. Interestingly, overexpression of LL-37 in mice prevents diet-induced increases in CD36 expression, hepatic steatosis and obesity (55). As Peptie 19-2.5 is a mimic of LL-37, its potential mechanism of action in models of diet-induced obesity, NASH and insulin resistance may be secondary to reduction of the expression of CD36. Hence, resulting in reduced lipid uptake. This may explain the observed reduction in weight gain, liver steatosis and the improvement in OGTT. Overall, our findings support the view that Peptide 19-2.5 prevents the upregulation of CD36 which is a significant driver in the pathogenesis of steatohepatitis.

There is good evidence that the expression of CD36 caused by HFD is secondary to the activation of the ERK1/2 (MAPK) pathway: Activation of ERK1/2 drives both CD36 expression and

lipid accumulation (56, 57), while inhibition of ERK1/2 activity reduces CD36 expression in hepatocytes (55). LL-37 inhibits ERK phosphorylation in macrophages (58) and the activation of ERK with EGF reverses both the inhibition of CD36 expression and the lipid accumulation caused by LL-37 in adipocytes and hepatocytes (55). We report here that Peptide 19-2.5 inhibits both the phosphorylation of ERK1/2 as well as CD36 expression caused by HFD in the liver. Taken together, these findings support the view that activation of ERK1/2 in the liver of mice subjected to a HFD drives the expression of CD36, which, in turn, promotes lipid deposition and ultimately steatohepatitis. The observed inhibition of ERK/1/2 phosphorylation in the liver of HFD-mice treated with Peptide 19-2.5, on the other hand, prevents expression of CD36, lipid deposition, liver inflammation and injury. Thus, like LL-37, Peptide 19-2.5, reduced CD36 expression through an ERK-dependent mechanism, which prevents lipid deposition in the liver of animals subjected to a HFD.

In addition to preventing the deposition of excessive fat in the liver (by inhibiting activation of ERK1/2 and the upregulation of CD36) and liver inflammation (by reducing the activation of NF-κB, iNOS expression and activation of the inflammasome), Peptide 19-2.5 may also reduce the degree of metabolic endotoxemia associated with HFD. There is good evidence that (a) HFD causes disruptions to tight junctions in the gut (59) (b) HFD causes the reduction in the expression of tight junctions (60) and (c) HFD causes the activation of NF-κB which regulates myosin light chain kinases (MLCK), and this increases tight junction permeability (61). Under healthy conditions the opening and closing of paracellular junction is tightly regulated allowing only digested proteins to pass through. However, dysregulation of the cellular junction by irritation from diet, stress or lack of exercise causes damage to the intestinal cells and the junctions loosen. It is the loss of barrier integrity that allows the translocation of LPS and undigested food particles *via* the mucosa to pass through into the bloodstream (62). This triggers an immune response leading to low-grade inflammation, as well as steatosis, insulin resistance and the secretion of cytokines. Endotoxins, for example LPS are able to interact with immune cells and adipocytes, leading to a chronic, systemic inflammation by activating NF-κB (e.g. in the liver) which importantly contributes to the development of met-inflammation. We report here that Peptide 19-2.5 attenuates the degree of phosphorylation of IKKα/β, IκBα, the translocation of NF-κB to the nucleus and the iNOS expression in the liver. These findings indicate that Peptide 19-2.5 may prevent the binding of LPS to TLR4 resulting in the prevention of the activation of NF-κB and the inflammasome. The lipid A moiety of LPS has a cubic aggregate structure and when bound to Peptide 19-2.5 is converted into an inactivated, multilamellar structure (14, 30). Atomic force imaging showed morphological changes of bacteria upon treatment with Peptide 19-2.5, with a strong ability to agglomerate the bacteria (46). The structure of the Peptide 19-2.5-LPS aggregate was determined using small-

angle-x-ray scattering (SAXS) (5). Freeze-fracture electron microscopy showed that LPS presents as a ribbon-like structures with a length of a few hundred μm and a thickness of 14-20 nm with varying width. In the presence of Peptide 19-2.5, the structure changes to large and more densely packed multilamellar aggregates (63). In the absence of Peptide 19-2.5 for peptide polymyxin B (PMB), there was no scattering signal. However, in the presence of Peptide 19-2.5 there was scattering between 22 nm and 25 nm and this value corresponds to the thickness of the bacterial envelope. The decrease in LPS bioactivity with the increased size of LPS aggregates is due to the fact that the binding sites for lipopolysaccharide binding protein (e.g. LBP) and CD14 are hidden in multilamellar aggregates. Interestingly, the binding affinity of the peptide exceeds that of other LPS-binding proteins (e.g LBP) and prevents the binding of LPS to TLR4 (64). Although both LL-37 and synthetic AMPs, such as Peptide 19-2.5, bind to and inactivate LPS, it should be noted that the effect of these cationic peptides is not limited to LPS alone, as they can also bind to lipoprotein (LP).

LP induces inflammation by activating TLR2 resulting in the activation of a signaling cascade that drives activation of NF-kB and, hence, the formation of many pro-inflammatory chemokines and cytokines (65). In skin cells, the AMPs Peptide 19-2.5 and Peptide 19-4LF inhibit the inflammatory response that is triggered by either LPS or LP (63). Cathelicidins are also capable of inhibiting inflammatory responses driven by TLR2 activation by directly interacting with TLR2 ligands (66). Using isothermal titration, LL-37 was shown to bind to lipoteichoic acid (LTA) and LPS (67). It has been proposed that the synthetic AMPs Peptide 19-2.5 and Peptide 19-4LF may also inhibit intracellular signaling events as well as the extracellular TLR2/4 signaling. This includes Peptide 19-2.5 inhibiting intracellular LPS-induced caspase-1 activation and HMGB1. Although the mechanism is unclear this may be due to Peptide 19-2.5 inhibiting extracellular LPS, hence preventing the accumulation intracellularly. TLR2 is also capable of initiating the activation of NLRP3 inflammasome (68).

Taken together, the above findings support the view that Peptide 19-2.5 may reduce the degree of diet-induced metabolic alterations by preventing metabolic endotoxemia. This potential mechanism of action is much more difficult to prove, as the determination of LPS in the blood (of the mesenteric or hepatic circulation) is difficult for a number of reasons: The limulus amebocyte lysate (LAL) assay is commonly used to detect endotoxins, but false positive results in blood obtained from animals subjected to a HFD may occur, as both triglycerides and very low-density lipoproteins increase the sensitivity of LAL assay, due to the direct activation of LAL. Patients with T2DM present higher levels of serum triglycerides, hence increasing the chance of false-positives (69). There is also a chance of false negatives results, as LPS entering the bloodstream allows the lipid A part of LPS to associate with the phospholipid of the serum lipoproteins, hence this will make it difficult to detect LPS using the LAL assay (70). These limitations are challenging to

overcome, however could use the LBP assay as well as the endotoxin activity assay (EAA) together with the LAL assay to confirm the results concluded (9, 71). Our finding here that an AMP which binds to and inactivates LPS reduces insulin-resistance, diabetic nephropathy and steatohepatitis supports the view that metabolic endotoxemia importantly contributes to their pathogenesis. This hypothesis is further supported by findings demonstrating that TLR-4 receptor deficient mice fed a HFD develop less insulin resistance (6, 7).

We have also used a metabolomic approach to gain a better insight into the effects of the HFD alone and presence of Peptide 19-2.5 on the metabolic phenotype of the animals: There is very good evidence that L-carnitine is involved in lipid metabolism and transports fatty acids into the mitochondria to increase the β-oxidation-mediated metabolism of fats in the liver (72). There is also good evidence that carnitine plays a role in maintaining liver function and is critical for choline metabolism. Our metabolome data showed that treatment of HFD-mice with peptide 19-2.5 restored serum carnitine level (which were lower in HFD-mice treated with vehicle). Carnitine is primarily synthesized from methionine and lysine in the liver and kidney and is important for the transport of fat into the mitochondria to generate ATP (26). Carnitine is also frequently used in supplements for weight loss and this could provide an explanation for the small reduction in weight loss in mice treated with Peptide 19-2.5 (73). Oral administration of L-carnitine improves insulin sensitivity in obese mice and reduces fasting glucose levels in patients with T2DM (74–76). In contrast, carnitine deficiency is associated with liver injury (77). We report here that mice challenged with HFD and treated with Peptide19-2.5 have restored serum levels of carnitine, which may have contributed to the beneficial effects of the AMP reported here.

Limitations of the Study

Adipose tissue macrophages can clear up dead adipocytes which accumulate during obesity. They can also internalize the excess free fatty acids which are released by insulin-resistant adipocytes which requires NOX2. $NOX^{-/-}$ mice in early diet-induced obesity shown an improvement of metabolic phenotypes, but this does worsen in late diet-induced obesity (78). Therefore, adipose tissue macrophages have shown to be critical in characterizing metabolic syndrome. This study has not addressed the impact of Peptide 19-2.5 on the activation of adipose tissue macrophages e.g. by LPS or LP (or other DAMPs or PAMPs known to play a role in the metabolic syndrome). Future studies are warranted to address this interesting and potentially important hypothesis.

CONCLUSIONS

There is good evidence that metabolic endotoxemia contributes to the pathophysiology of obesity, metaflammation and diabetes. We report here for the first time that patients with T2DM have elevated levels of the human cathelicidin LL-37. The effects of

LPS-binding proteins in experimental diabetes have not yet been investigated. To gain a better understanding of the role of LPS-binding AMPs in the pathophysiology of diabetes, we have challenged mice with a HFD for 12 weeks in the presence and absence of the LPS-binding protein, Pep2-5. We report here for the first time that Peptide 19-2.5 attenuates the IRS-1 phosphorylation in the liver, diabetic nephropathy (proteinuria), hypercholesterolemia and steatohepatitis caused by HFD in the mouse. The reductions in liver fat deposition (liver weight and staining for fat) and steatohepatitis (reduced activation of NF-κB, inflammasome and release of ALT) observed in HFD-mice treated with Peptide 19-2.5 are, at least in part, due to reduced expression of CD36 secondary to inhibition of ERK-1/2 in the liver. Although difficult to prove, a reduction in the degree of metabolic endotoxemia may also have importantly contributed to the observed beneficial effects of Peptide 19-2.5 in mice challenged with a HFD.

DATA AVAILABILITY STATEMENT

The original contributions presented in the study are included in the article/**Supplementary Material**. Further inquiries can be directed to the corresponding authors.

ETHICS STATEMENT

AUTHOR CONTRIBUTIONS

SM, SAZ, ES, MMY, SMC, LM and CT conceived and designed the experiments. SM, SAZ, DC, NK, BW and GFA performed the experiments. SM, SAZ, GDN, AB, ALC, MC, NK, BW SMC, WC-V and CT analyzed the data. SM, KB, SMC, NK, MMY, LM and CT contributed to the writing of the manuscript. All authors reviewed and approved the submitted version.

FUNDING

ACKNOWLEDGMENTS

SUPPLEMENTARY MATERIAL

The Supplementary Material for this article can be found online at: https://www.frontiersin.org/articles/10.3389/fimmu.2021. 701275/full#supplementary-material

REFERENCES

1. Chelakkot C, Ghim J, Ryu SH. Mechanisms Regulating Intestinal Barrier Integrity and Its Pathological Implications. *Exp Mol Med* (2018) 50(8):1–9. doi: 10.1038/s12276-018-0126-x

2. Vancamelbeke M, Vermeire S. The Intestinal Barrier: A Fundamental Role in Health and Disease. *Expert Rev Gastroenterol Hepatol* (2017) 11(9):821–34. doi: 10.1080/17474124.2017.1343143

3. Pålsson-McDermott EM, O'Neill LA. Signal Transduction by the Lipopolysaccharide Receptor, Toll-Like Receptor-4. *Immunology* (2004) 113 (2):153–62. doi: 10.1111/j.1365-2567.2004.01976.x

4. Cani PD, Amar J, Iglesias MA, Poggi M, Knauf C, Bastelica D, et al. Metabolic Endotoxemia Initiates Obesity and Insulin Resistance. *Am Diabetes Assoc* (2007) 56(7):1761–72. doi: 10.2337/db06-1491

5. Boutagy NE, McMillan RP, Frisard MI, Hulver MW. Metabolic Endotoxemia With Obesity: Is it Real and Is it Relevant? *Biochimie* (2016) 124:11–20. doi: 10.1016/j.biochi.2015.06.020

6. Lee JJ, Wang PW, Yang IH, Huang HM, Chang CS, Wu CL, et al. High-Fat Diet Induces Toll-Like Receptor 4-Dependent Macrophage/Microglial Cell Activation and Retinal Impairment. *Invest Ophthalmol* (2015) 56(5):3041– 50. doi: 10.1167/iovs.15-16504

7. Jia L, Vianna CR, Fukuda M, Berglund ED, Liu C, Tao C, et al. Hepatocyte Toll-Like Receptor 4 Regulates Obesity-Induced Inflammation and Insulin Resistance. *Nat Commun* (2014) 5:3878. doi: 10.1038/ncomms4878

8. Björkbacka H, Kunjathoor VV, Moore KJ, Koehn S, Ordija CM, Lee MA, et al. Reduced Atherosclerosis in MyD88-Null Mice Links Elevated Serum Cholesterol Levels to Activation of Innate Immunity Signaling Pathways. *Nat Med* (2004) 10(4):416–21. doi: 10.1038/nm1008

9. Mohammad S, Thiemermann C. Role of Metabolic Endotoxemia in Systemic Inflammation and Potential Interventions. *Front Immunol* (2021) 11:1–16. doi: 10.3389/fimmu.2020.594150

10. Rubler S, Dlugash J, Yuceoglu YZ, Kumral T, Branwood A, Grishman A. New Type of Cardiomyopathy Associated With Diabetic Glomerulosclerosis. *Am J Cardiol* (1872) 30(6):595–602. doi: 10.1016/0002-9149(72)90595-4

11. Koonen DP, Jacobs RL, Febbraio M, Young ME, Soltys CL, Ong H, et al. Increased Hepatic CD36 Expression Contributes to Dyslipidemia Associated With Diet-Induced Obesity. *Diabetes* (2007) 56(12):2863–71. doi: 10.2337/ db07-0907

12. Braster Q, Silvestre-Roig C, Hartwig H, Kusters P, Aarts S, den Toom M, et al. Cathelicidin Regulates Myeloid Cell Accumulation in Adipose Tissue and Promotes Insulin Resistance During Obesity. *Thromb Haemost* (2016) 115 (6):1237–9. doi: 10.1160/TH16-02-0112

13. Kahlenberg JM, Kaplan MJ. Little Peptide, Big Effects: The Role of LL-37 in Inflammation and Autoimmune Disease. *J Immunol* (2013) 191(10):4895– 901. doi: 10.4049/jimmunol.1302005

14. Kaconis Y, Kowalski I, Howe J, Brauser A, Richter W, Olazaran IR, et al. Biophysical Mechanisms of Endotoxin Neutralization by Cationic Amphiphilic Peptides. *Biophys J* (2011) 100(11):2652–61. doi: 10.1016/ j.bpj.2011.04.041

15. Martin L, Horst K, Chiazza F, Oggero S, Collino M, Brandenburg K, et al. The Synthetic Antimicrobial Peptide 19-2.5 Attenuates Septic Cardiomyopathy and Prevents Down-Regulation of SERCA2 in Polymicrobial Sepsis. *Sci Rep* (2016) 6:37277. doi: 10.1038/srep37277

16. Fracanzani AL, Pisano G, Consonni D, Tirabosci S, Baragetti A, Bertelli C, et al. Epicardial Adipose Tissue (EAT) Thickness Is Associated With Cardiovascular and Liver Damage in Nonalcoholic Fatty Liver Disease. *PloS One* (2016) 11(9):1–19. doi: 10.1371/journal.pone.0162473

17. Baragetti A, Severgnini M, Olmastroni E, Dioguardi CC, Mattavelli E, Angius A, et al. Gut Microbiota Functional Dysbiosis Relates to Individual Diet in Subclinical Carotid Atherosclerosis. *Nutrients* (2021) 13(2):1–19. doi: 10.3390/nu13020304

18. Baragetti A, Palmen J, Garlaschelli K, Grigore L, Humphries SE, Talmud PJ, et al. Genetically Determined Telomeres Shortening Is Associated With Carotid Atherosclerosis Progression and Increased Incidence of Cardiovascular Events. *Int J Cardiol* (2016) 223:43–5. doi: 10.1016/ j.ijcard.2016.08.164

19. Alberti KGMM, Eckel RH, Grundy SM, Zimmet PZ, Cleeman JI, Donato KA, et al. Harmonizing the Metabolic Syndrome: A Joint Interim Statement of the International Diabetes Federation Task Force on Epidemiology and Prevention; National Heart, Lung, and Blood Institute; American Heart Association; World Heart Federation; International. *Circulation* (2009) 120 (16):1640–45. doi: 10.1161/CIRCULATIONAHA.109.192644

20. Davies MJ, D'Alessio DA, Fradkin J, Keran WN, Mathieu C, Mingrone G, et al. Management of Hyperglycemia in Type 2 Diabetes. A Consensus Report by the American Diabetes Association (ADA) and the European Association for the Study of Diabetes (EASD). *Diabetes Care* (2018) 41(12):2669–701. doi: 10.2337/dci18-0033

21. Baragetti A, Norata GD, Sarcina C, Rastelli F, Grigore L, Garlaschelli K, et al. High Density Lipoprotein Cholesterol Levels Are an Independent Predictor of the Progression of Chronic Kidney Disease. *J Intern Med* (2013) 274(3):252– 62. doi: 10.1111/joim.12081

22. Benjamini Y, Hochberg Y. Controlling the False Discovery Rate: A Practical and Powerful Approach to Multiple Testing. *J R Stat Soc Series B* (1995) 57 (1):289–300. doi: 10.1111/j.2517-6161.1995.tb02031.x

23. Viana LV, Gross JL, Camargo JL, Zelmanovitz T, da Costa Rocha EP, Azevedo MJ. Prediction of Cardiovascular Events, Diabetic Nephropathy, and Mortality by Albumin Concentration in a Spot Urine Sample in Patients With Type 2 Diabetes. *J Diabetes Complications* (2012) 26(5):407–12. doi: 10.1016/j.jdiacomp.2012.04.014

24. Mattix HJ, Hsu CY, Shaykevich S, Curhan G. Use of the Albumin/Creatinine Ratio to Detect Microalbuminuria: Implications of Sex and Race. *J Am Soc Nephrol* (2002) 13(4):1034–9. doi: 10.1681/ASN.V1341034

25. Velázquez KT, Enos RT, Bader JE, Sougiannis AT, Carson MS, Chatzistamou I, et al. Prolonged High-Fat-Diet Feeding Promotes Non-Alcoholic Fatty Liver Disease and Alters Gut Microbiota in Mice. *World J Hepatol* (2019) 11 (8):619–37. doi: 10.4254/wjh.v11.i8.619

26. Mingrone G. Carnitine in Type 2 Diabetes. *Ann N Y Acad Sci* (2004) 1033:99– 107. doi: 10.1196/annals.1320.009

27. Johansson J, Gudmundsson GH, Rottenberg ME, Berndt K, Agerberth B. Conformation-Dependent Antibacterial Activity of the Naturally Occurring Human Peptide LL-37. *J Biol Chem* (1998) 273(6):3718–24. doi: 10.1074/jbc.273.6.3718

28. Fukumoto K, Dewanjee MK, Kaye MP, Josa M, Metke MP, Chesbro JH. Effect of Antibacterial Catelicidin Peptide CAP18/LL-37 on Sepsis in Neonatal Rats. *Pediatr Surg Int* (2005) 21(1):20–4. doi: 10.1007/s00383-004-1256-x

29. Martin L, Santis R, Koczera P, Simons N, Haase H, Heinbockel L, et al. The Synthetic Antimicrobial Peptide 19-2.5 Interacts With Heparanase and Heparan Sulfate in Murine and Human Sepsis. *PloS One* (2015) 10(11):e0143583. doi: 10.1371/journal.pone.0143583

30. Gutsmann T, Olazaran IR, Kowalski I, Kaconis Y, Howe J, Bartels R, et al. New Antiseptic Peptides to Protect Against Endotoxin-Mediated Shock. *Antimicrob Agents Chemother* (2010) 54(9):3817–24. doi: 10.1128/AAC.00534-10

31. Winzell MS, Ahren B. The High-Fat Diet-Fed Mouse: A Model for Studying Mechanisms and Treatment of Impaired Glucose Tolerance and Type 2 Diabetes. *Diabetes* (2004) 53(3):S215–19. doi: 10.2337/diabetes.53.suppl_3.S215

32. Gao Z, Hwang D, Bataille F, Lefevre M, York D, Quon MJ, et al. Serine Phosphorylation of Insulin Receptor Substrate 1 by Inhibitor κB Kinase Complex. *J Biol Chem* (2002) 277(50):48115–21. doi: 10.1074/jbc.M209459200

33. Dabla PK. Renal Function in Diabetic Nephropathy. *World J Diabetes* (2010) 1(2):48. doi: 10.4239/wjd.v1.i2.48

34. Aldukhayel A. Prevalence of Diabetic Nephropathy Among Type 2 Diabetic Patients in Some of the Arab Countries. *Int J Health Sci (Qassim)* (2017) 11(1):1–4.

35. O'brien PD, Sakowski SA, Feldman EL. Mouse Models of Diabetic Neuropathy. *ILAR J* (2014) 54(3):259–72. doi: 10.1093/ilar/ilt052

36. Palsson R, Patel UD. Cardiovascular Complications of Diabetic Kidney Disease. *Adv Chronic Kidney Dis* (2015) 21(3):273–80. doi: 10.1053/j.ackd.2014.03.003

37. Noh H, King GL. The Role of Protein Kinase C Activation in Diabetic Nephropathy. *Kidney Int* (2007) (SUPPL. 106):S49–53. doi: 10.1038/sj.ki.5002386

38. Gao M, Ma Y, Liu D. High-Fat Diet-Induced Adiposity, Adipose Inflammation, Hepatic Steatosis and Hyperinsulinemia in Outbred CD-1 Mice. *PloS One* (2015) 10(3):1–15. doi: 10.1371/journal.pone.0119784

39. Luedde T, Schwabe RF. NF-[Kappa]B in the Liver–Linking Injury, Fibrosis and Hepatocellular Carcinoma. *Nat Rev Gastroenterol Hepatol* (2011) 8(2):108–18. doi: 10.1038/nrgastro.2010.213

40. Wan X, Xu C, Yu C, Li Y. Role of NLRP3 Inflammasome in the Progression of NAFLD to NASH. *Can J Gastroenterol Hepatol* (2016) 2016:6489012. doi: 10.1155/2016/6489012

41. Cai D, Yuan M, Frantz DF, Melendez PA, Hansen L, Lee J, et al. Local and Systemic Insulin Resistance Resulting From Hepatic Activation of IKK-β and NF-kB. *Nat Med* (2005) 11:(2):183–90. doi: 10.1038/nm1166

42. Salvatore P, Concetta B, Francesca Z, Franzoso G. Mechanisms of Liver Disease: The Crosstalk Between the NF-κB and JNK Pathways. *Biol Chem* (2010) 390(10):965–76. doi: 10.1515/BC.2009.111

43. Bharrhan S, Chopra K, Arora SK, Toor JS, Rishi P. Down-Regulation of NF-κB Signalling by Polyphenolic Compounds Prevents Endotoxin-Induced Liver Injury in a Rat Model. *Innate Immun* (2012) 18(1):70–9. doi: 10.1177/1753425910393369

44. Fujimoto M, Shimizu N, Kunii K, Martyn JA, Ueki K, Kaneki M. A Role for iNOS in Fasting Hyperglycemia and Impaired Insulin Signaling in the Liver of Obese Diabetic Mice. *Diabetes* (2005) 54(5):1340–8. doi: 10.2337/diabetes.54.5.1340

45. Perreault M, Marette A. Targeted Disruption of Inducible Nitric Oxide Synthase Protects Against Obesity-Linked Insulin Resistance in Muscle. *Nat Med* (2002) 7(10):1138–43. doi: 10.1038/nm1001-1138

46. Wree A, Mcgeough MD, Pena CA, Schlattjan M, Li H, Inzaugarat ME, et al. NLRP3 Inflammasome Activation Is Required for Fibrosis Development in NAFLD. *J Mol Med* (2014) 92(10):1069–82. doi: 10.1007/s00109-014-1170-1

47. Mridha AR, Wree A, Robertson AAB, Yeh MM, Johnson CD, Rooyen DMV, et al. NLRP3 Inflammasome Blockade Reduces Liver Inflammation and Fibrosis in Experimental NASH in Mice. *J Hepatol* (2017) 66(5):1037–46. doi: 10.1016/j.jhep.2017.01.022

48. Wree A, McGeough MD, Inzaugarat ME, Eguchi A, Schuster S, Johnson CD, et al. NLRP3 Inflammasome Driven Liver Injury and Fibrosis: Roles of IL-17 and TNF in Mice. *Hepatology* (2018) 67(2):736–49. doi: 10.1002/hep.29523

49. Ress C, Kaser S. Mechanisms of Intrahepatic Triglyceride Accumulation,". *World J Gastroenterol* (2016) 22(4):1664–73. doi: 10.3748/wjg.v22.i4.1664

50. Wilson CG, Tran TL, Erion DM, Vera NB, Febbraio M, Weiss EJ. Hepatocyte-Specific Disruption of CD36 Attenuates Fatty Liver and Improves Insulin Sensitivity in HFD-Fed Mice. *Endocrinology* (2016) 157(2):570–85. doi: 10.1210/en.2015-1866

51. Alkhatatbeh MJ, Enjeti AN, Acharya S, Thorne RF, Lincz LF. The Origin of Circulating CD36 in Type 2 Diabetes. *Nutr Diabetes* (2013) 3(2):e59. doi: 10.1038/nutd.2013.1

52. Kennedy DJ, Kashyap SR. Pathogenic Role of Scavenger Receptor CD36 in the Metabolic Syndrome and Diabetes. *Metab Syndr Relat Disord* (2011) 9(4):239–45. doi: 10.1089/met.2011.0003

53. Puchałowicz K, Rać ME. The Multifunctionality of CD36 in Diabetes Mellitus and Its Complications-Update in Pathogenesis, Treatment and Monitoring. *Cells* (2020) 9(8):1877. doi: 10.3390/cells9081877

54. Hui ST, Parks BW, Org E, Norheim F, Che N, Pan C, et al. The Genetic Architecture of NAFLD Among Inbred Strains of Mice. *Elife* (2015) 4:e05607. doi: 10.7554/eLife.05607

55. Tran DH, Tran DH, Mattai SA, Sallam T, Ortiz C, Lee EC, et al. Cathelicidin Suppresses Lipid Accumulation and Hepatic Steatosis by Inhibition of the CD36 Receptor. *Int J Obes* (2016) 40(9):1424–34. doi: 10.1038/ijo.2016.90

56. Turcotte LP, Raney MA, Todd MK. ERK1/2 Inhibition Prevents Contraction-Induced Increase in Plasma Membrane FAT/CD36 Content and FA Uptake in Rodent Muscle. *Acta Physiol Scand* (2005) 184(2):131–9. doi: 10.1111/j.1365-201X.2005.01445.x

57. Sini S, Deepa D, Harikrishnan S, Jayakumari N. High-Density Lipoprotein From Subjects With Coronary Artery Disease Promotes Macrophage Foam Cell Formation: Role of Scavenger Receptor CD36 and ERK/MAPK Signaling. *Mol Cell Biochem* (2017) 427(1-2):23–34. doi: 10.1007/s11010-016-2895-7

58. Fabiano PS, Richard LG. Differing Effects of Exogenous or Endogenous Cathelicidin on Macrophage Toll-Like Receptor Signaling. *Immunol Cell Biol* (2009) 87(60):496–500. doi: 10.1038/icb.2009.19

59. Ahmad R, Rah B, Bastola D, Dhawan P, Singh AB. Obesity-Induces Organ and Tissue Specific Tight Junction Restructuring and Barrier Deregulation by Claudin Switching. *Sci Rep* (2017) 7(1):1–16. doi: 10.1038/s41598-017-04989-8

60. Kim KA, Gu W, Lee IA, Joh EA, Kim DH. Hiigh Fat Diet-Induced Gut Microbiota Exacerbates Inflammation and Obesity in Mice Via the TLR4 Signaling Pathway. *PloS One* (2012) 7(10):e7713. doi: 10.1371/journal.pone.0047713

61. He WQ, Wang J, Sheng JY, Zha JM, Graham WV, Turner JR. Contributions of Myosin Light Chain Kinase to Regulation of Epithelial Paracellular Permeability and Mucosal Homeostasis. *Int J Mol Sci* (2020) 21(3):993. doi: 10.3390/ijms21030993

62. Awad WA, Hess C, Hess M. Enteric Pathogens and Their Toxin-Induced Disruption of the Intestinal Barrier Through Alteration of Tight Junctions in Chickens. *Toxins (Basel)* (2017) 9(2):60. doi: 10.3390/toxins9020060

63. Correa W, Heinbockel L, Behrends J, Kaconis Y, Varela S, Gutsmann T, et al. Antibacterial Action of Synthetic Antilipopolysaccharide Peptides (SALP) Involves Neutralization of Both Membrane-Bound and Free Toxins. *FEBS J* (2019) 286(8):1576–93. doi: 10.1111/febs.14805

64. Brandenburg K, Heinbockel L, Correa W, Lohner K. Peptides With Dual Mode of Action: Killing Bacteria and Preventing Endotoxin-Induced Sepsis. *Biochim Biophys Acta - Biomembr* (2016) 1858(5):71–979. doi: 10.1016/j.bbamem.2016.01.011

65. Heinbockel L, Weindl G, Martinez-de-Tejada G, Correa W, Sanchez-Gomez S, Bárcena-Varela S, et al. Inhibition of Lipopolysaccharide- and Lipoprotein-Induced Inflammation by Antitoxin Peptide Pep19-2.5. *Front Immunol* (2018) 9:1–6. doi: 10.3389/fimmu.2018.01704

66. Scheenstra MR, vVan Harten RM, Veldhuizen EJA, Haagsman HP, Coorens M. Cathelicidins Modulate TLR-Activation and Inflammation. *Front Immunol* (2020) 11:1–16. doi: 10.3389/fimmu.2020.01137

67. Schneider VAF, Coorens M, Ordonez SR, Bokhoven JLMT, Posthuma G, Dijk AV, et al. Imaging the Antimicrobial Mechanism(s) of Cathelicidin-2. *Sci Rep* (2016) 6:1–11. doi: 10.1038/srep32948

68. Wu HM, Zhao CC, Xie QM, Xu J, Fei GGH. TLR2-Melatonin Feedbck Loop Regulates the Activation of NLRP3 Inflammasome in Murine Allergic Airway Inflammation. *Front Immunol* (2020) 7(11):172. doi: 10.3389/fimmu.2020.00172

69. Al-Attas OS, Daghri NM, Rubeaan K, de Silva NF, Sabico SL, Kumar S, et al. Changes in Endotoxin Levels in T2DM Subjects on Anti-Diabetic Therapies. *Cardiovasc Diabetol* (2009) 8(1):20. doi: 10.1186/1475-2840-8-20

70. Berbée JFP, Havekes LM, Rensen PCN. Apolipoproteins Modulate the Inflammatory Response to Lipopolysaccharide. *J Endotoxin Res* (2005) 11(2):97–103. doi: 10.1179/096805105X35215

71. Pearce K, Estanislao D, Fareed S, Tremellen K. Metabolic Endotoxemia, Feeding Studies and the Use of the Limulus Amebocyte (LAL) Assay; Is it Fit for Purpose? *Diagnostics (Basel)* (2020) 10(6):428. doi: 10.3390/diagnostics10060428

72. Fujisawa F, Takami T, Matsuzaki A, Matsumoto T, Yamamoto N, Terai S, et al. Evaluation of the Effects of L-Carnitine on Medaka (Oryzias Latipes) Fatty Liver. *Sci Rep* (2017) 7(1):1–10. doi: 10.1038/s41598-017-02924-5

73. Pooyandjoo M, Nouhi M, Shab-Bidar S, Djafarian K, Olyaeemanesh A. The Effect of (L-)Carnitine on Weight Loss in Adults: A Systematic Review and Meta-Analysis of Randomized Controlled Trials. *Obes Rev* (2016) 17(10):970–76. doi: 10.1111/obr.12436

74. Galloway SDR, Craig TP, Cleland SJ. Effects of Oral L-Carnitine Supplementation on Insulin Sensitivity Indices in Response to Glucose Feeding in Lean and Overweight/Obese Males. *Amino Acids* (2011) 41(2):507–15. doi: 10.1007/s00726-010-0770-5

75. Rahbar AR, Shakerhosseini R, Saadat N, Taleban F, Pordal A, Gollestan B. Effect of L-Carnitine on Plasma Glycemic and Lipidemic Profile in Patients With Type II Diabetes Mellitus. *Eur J Clin Nutr* (2005) 59(4):592–96. doi: 10.1038/sj.ejcn.1602109

76. Pirmadah F, Ramezani-Jolfaie N, Mohammadi M, Talenezhad N, Clark CCT, Abargouei AS. Does L-Carnitine Supplementation Affect Serum Levels of Enzymes Mainly Produced by Liver? A Systematic Review and Meta-Analysis of Randomized Controlled Clinical Trials. *Eur J Nutr* (2021) 59(5):1767–83. doi: 10.1007/s00394-019-02068-4

77. Cave MC, Hurt RT, Frazier TH, Matheson PJ, Garrison RN, McClain CJ, et al. Obesity, Inflammation, and the Potential Application of Pharmaconutrition. *Nutr Clin Pract* (2008) 23(1):16–34. doi: 10.1177/011542650802300116

78. Coats BR, Schoenfelt KQ, Barbosa-Lorenzi VC, Peris E, Cui C, Hoffman A, et al. Metabolically Activated Adipose Tissue Macrophages Perform Detrimental and Beneficial Functions During Diet-Induced Obesity. *Cell Rep* (2017) 20(13):3149–61. doi: 10.1016/j.celrep.2017.08.096

Conflict of Interest: The authors declare that the research was conducted in the absence of any commercial or financial relationships that could be construed as a potential conflict of interest.